Hybridizable Discontinuous Galerkin method for the simulation of the propagation of the elastic wave equations in the frequency domain

Marie Bonnasse-Gahot, Henri Calandra, Julien Diaz, Stéphane Lanteri

Hybridizable Discontinuous Galerkin method for the simulation of the propagation of the elastic wave equations in the frequency domain

Marie Bonnasse-Gahot, Henri Calandra, Julien Diaz, Stéphane Lanteri

RESEARCH REPORT

N° 8990

June 2015

Project-Teams Magique 3D and Nachos

ISSN 0249-6399 ISRN INRIA/RR--8990--FR+ENG

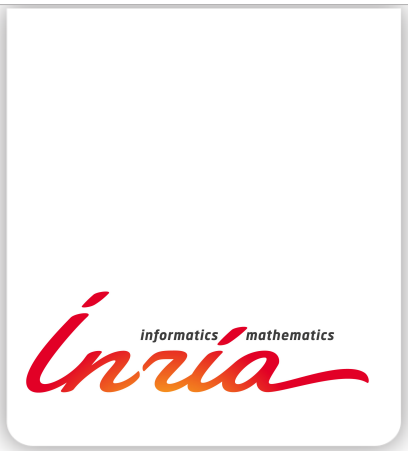

Hybridizable Discontinuous Galerkin method for the simulation of the propagation of the elastic wave equations in the frequency domain

Marie Bonnasse-Gahot*†, Henri Calandra‡, Julien Diaz*, Stéphane Lanteri †

Project-Teams Magique 3D and Nachos

Research Report n° 8990 — June 2015 — 43 pages

Abstract: In this report, we study the hybridizable discontinuous Galerkin (HDG) method for the resolution of the 2D elastic waves equations in frequency domain, so called Helmholtz equations. We give the formulation of the method and we compare the obtained results to a nodal discontinuous Galerkin (DG) method : the upwind flux DG method.

Key-words: seismic imaging, forward problem, frequency domain, elastic waves, Hybridizable DG method, discontinuous Galerkin method

* EPI Magique 3D INRIA Bordeaux-Sud-Ouest
† EPI Nachos INRIA Sophia Antipolis-Méditerranée
‡ TOTAL Exploration-Production

RESEARCH CENTRE BORDEAUX – SUD-OUEST

200 avenue de la Vieille Tour
33405 Talence Cedex

Méthode de Galerkine discontinue hybride pour les équations d'Helmholtz élastiques

Résumé : Dans ce rapport, nous étudions la méthode Galerkine discontinue hybride (GDH) pour la résolution des équations 2D des ondes élastiques en domaine fréquentiel, appelées aussi équations d'Helmholtz élastiques. Nous présentons la formulation de la méthode et nous comparons les résultats numériques á une méthode Galerkine discontinue nodale: la méthode GD à flux décentrés.

Mots-clés : imagerie sismique, résolution du problème direct, domain fréquentiel,ondes élastiques, méthodes de Galerkin discontinues, méthode GD hybride

Contents

1 Introduction

Discontinuous Galerkin (DG) methods have been studied for a lot of problems, particularly in time-domain where they give suitable results. They present a lot of advantages among which a high flexibility to the type of mesh used for discretizing complex geometries, *hp*-adaptativity (i.e. local adaptation of the discretization parameter and interpolation degree) and easy parallelization. Their main drawback is their computational cost (CPU time and memory) as compared to classical (continuous) finite element (CG) methods because they incur additional degrees of freedom, especially when an arbitrarily high order interpolation of the field components is used. This is due to the fact that the degrees of freedom belong to only one element (because basis functions are discontinuous at the interfaces of the elements) and so, the degrees of freedom placed at the interfaces have to be duplicated. As a consequence, DG methods lead to larger sparse linear systems with a higher number of globally coupled degrees of freedom as compared to CG methods on the same given mesh.

To get around this drawback, we consider here a new DG method: the hybridizable DG method (HDG) (see [1] for more details). The basic principle of this HDG method consists in introducing a Lagrange multiplier representing the trace of the numerical solution on each face of the mesh cells. This new variable exists only on the faces of the mesh and the unknowns of the problem depend on it. This allows us to reduce the number of globally coupled unknowns and

thus the number of degrees of freedom of the global linear system. Now the size of the matrix to be inverted only depends on the number of degrees of freedom of each face and the number of faces of the mesh. It is worth noting that for a nodal DG method, this size depends on the number of degrees of freedom of each element and on the number of elements of the mesh. Finally the solution of the initial problem is recovered thanks to a simple linear independent elementwise calculation. Moreover, the parallelization of the HDG formulation does not induce any additional difficulty in comparison with classical DG methods.

The HDG method has been introduced in [2] for a model second order elliptic problem. Recently it has been applied for many problems such as for the time-domain elastodynamic equations time integrated implicitly [3], the frequency-domain Maxwell Maxwell equations [4]-[5], convection-diffusion problems [6]-[7] or fluid flow problems [8]. To the best of our knownledge, there is no similar work for the solution of the frequency-domain elastodynamic equations. This report is divided in four main sections. We first present the problem that we consider and the notations that we used in our work. The second part describes the nodal centered and upwind DG methods that we previously developped in [9]. In the remaining parts, the upwind DG method is used to be a reference method to which we compare the HDG method results. The third part explains the HDG formulation for the 2D elastic Helmholtz equations, while the last part is dedicated to numerical results.

2 Problem statement and notations

2.1 Time-harmonic 2D elastic wave equations

We consider the first order formulation of the 2D elastic wave equations in harmonic domain. We have, for $\mathbf{x} = (x, z) \in \Omega \subset \mathbb{R}^2$

$$\left\{ \begin{array}{lcll} i\omega\rho(\mathbf{x})\mathbf{v}(\mathbf{x}) & = & \nabla \cdot \underline{\underline{\sigma}}(\mathbf{x}) + f(\mathbf{x}) & \text{in } \Omega, \\ i\omega\underline{\underline{\sigma}}(\mathbf{x}) & = & \underline{\underline{C}}(\mathbf{x}) \ \underline{\underline{\epsilon}}(\mathbf{v}(\mathbf{x})) & \text{in } \Omega, \end{array} \right. \tag{2.1}$$

where i is the imaginary unit, ω the angular frequency. Then $\rho(\mathbf{x})$ defines the mass density and $f(\mathbf{x})$ the source term, which is generally associated to volumic forces. The vector $\mathbf{v}(\mathbf{x}) = (\ v_x(\mathbf{x}),\ \ v_z(\mathbf{x})\ )^T$ is the velocity vector and $\underline{\underline{\epsilon}}$ the strain tensor, where $\epsilon_{ij} = \frac{1}{2}\left(\frac{\partial v_i}{\partial j} + \frac{\partial v_j}{\partial i}\right), \quad i, j = x, z.$ $\underline{\underline{\sigma}}$ is the stress tensor; in the general case, $\sigma_{ij} = \sum_{k=1}^{2}\sum_{l=1}^{2} C_{ijkl}\epsilon_{kl}$ and in the particular isotropic case, $\sigma_{ij} = \lambda\delta_{ij}tr(\underline{\underline{\epsilon}}) + 2\mu\epsilon_{ij}, \quad i, j = x, z$, with λ and μ Lame's coefficients. The tensor $\underline{\underline{C}}$ is a fourth order symetric tensor contening the elastic coefficients. Using Voigt's notation, we reduce it to a 3×3 matrix

$$\begin{aligned} ij \to \alpha \text{ or } kl \to \beta = 11 &\to 1, \\ 22 &\to 2, \\ 12 &\to 3. \end{aligned}$$

In the general anisotropic case we have

$$\underline{\underline{C}}(\mathbf{x}) = \begin{pmatrix} C_{11} & C_{12} & C_{13} \\ C_{12} & C_{22} & C_{23} \\ C_{13} & C_{23} & C_{33} \end{pmatrix},$$

while in the isotropic case

$$\underline{\underline{C}}(\mathbf{x}) = \begin{pmatrix} \lambda(\mathbf{x}) + 2\mu(\mathbf{x}) & \lambda(\mathbf{x}) & 0 \\ \lambda(\mathbf{x}) & \lambda(\mathbf{x}) + 2\mu(\mathbf{x}) & 0 \\ 0 & 0 & \mu(\mathbf{x}) \end{pmatrix}.$$

Thereafter we do not write space dependencies for physical parameters ρ, λ and μ, tensors $\underline{\underline{C}}, \underline{\underline{\sigma}}$ and $\underline{\underline{\epsilon}}$ and for the vector $\mathbf{v}$ and we assume that physical parameters (ρ, λ and μ for the isotropic case and ρ and the C_{ij} coefficients in the general case) are piecewise constant.

We can develop the equations of the system (2.1).
In the anisotropic case, we have for $(x, z) \in \Omega \subset \mathbb{R}^2$:

$$\left\{ \begin{array}{rcl} i\omega v_x &=& \dfrac{1}{\rho}\left(\dfrac{\partial \sigma_{xx}}{\partial x} + \dfrac{\partial \sigma_{xz}}{\partial z}\right) + f_x, \\ i\omega v_z &=& \dfrac{1}{\rho}\left(\dfrac{\partial \sigma_{xz}}{\partial x} + \dfrac{\partial \sigma_{zz}}{\partial z}\right) + f_z, \\ i\omega \sigma_{xx} &=& C_{11}\dfrac{\partial v_x}{\partial x} + C_{12}\dfrac{\partial v_z}{\partial z} + C_{13}\left(\dfrac{\partial v_x}{\partial z} + \dfrac{\partial v_z}{\partial x}\right), \\ i\omega \sigma_{zz} &=& C_{12}\dfrac{\partial v_x}{\partial x} + C_{22}\dfrac{\partial v_z}{\partial z} + C_{23}\left(\dfrac{\partial v_x}{\partial z} + \dfrac{\partial v_z}{\partial x}\right), \\ i\omega \sigma_{xz} &=& C_{13}\dfrac{\partial v_x}{\partial x} + C_{23}\dfrac{\partial v_z}{\partial z} + C_{33}\left(\dfrac{\partial v_x}{\partial z} + \dfrac{\partial v_z}{\partial x}\right), \end{array} \right. \tag{2.2}$$

and for the isotropic case, we have for $(x, z) \in \Omega \subset \mathbb{R}^2$:

$$\left\{ \begin{array}{rcl} i\omega v_x &=& \dfrac{1}{\rho}\left(\dfrac{\partial \sigma_{xx}}{\partial x} + \dfrac{\partial \sigma_{xz}}{\partial z}\right) + f_x, \\ i\omega v_z &=& \dfrac{1}{\rho}\left(\dfrac{\partial \sigma_{xz}}{\partial x} + \dfrac{\partial \sigma_{zz}}{\partial z}\right) + f_z, \\ i\omega \sigma_{xx} &=& (\lambda + 2\mu)\dfrac{\partial v_x}{\partial x} + \lambda\dfrac{\partial v_z}{\partial z}, \\ i\omega \sigma_{zz} &=& \lambda\dfrac{\partial v_x}{\partial x} + (\lambda + 2\mu)\dfrac{\partial v_z}{\partial z}, \\ i\omega \sigma_{xz} &=& \mu\left(\dfrac{\partial v_x}{\partial z} + \dfrac{\partial v_z}{\partial x}\right). \end{array} \right. \tag{2.3}$$

The boundary conditions are given by

$$\underline{\underline{\sigma}} \cdot \mathbf{n} = 0 \quad \text{on } \Gamma_l, \tag{2.4}$$

$$\underline{\underline{\sigma}} \cdot \mathbf{n} + PA(\theta')P^T\mathbf{v} = 0 \quad \text{on } \Gamma_a, \tag{2.5}$$

where $\Gamma_l \cup \Gamma_a = \partial\Omega$ and $\Gamma_l \cap \Gamma_a = \emptyset$, $v_p = \sqrt{\dfrac{\lambda + 2\mu}{\rho}}$ is the P-wave velocity, $v_s = \sqrt{\dfrac{\mu}{\rho}}$ the S-wave velocity, $\mathbf{n}$ the outward unit norm vector and $\mathbf{t}$ the unit tangent. Relation (2.4) defines a free surface condition whereas (2.5) represent an absorbing boundary condition in the anisotropic case. The matrices P, $A(\theta)$ and θ' will be defined in section 4.3. In the isotropic case, the condition (2.5) is reduced to

$$\underline{\underline{\sigma}} \cdot \mathbf{n} - \rho v_p(\mathbf{v} \cdot \mathbf{n})\mathbf{n} + \rho v_s(\mathbf{v} \cdot \mathbf{t})\mathbf{t} = 0 \text{ on } \Gamma_a \tag{2.6}$$

2.2 Notations

We consider a triangulation $\mathcal{T}_h$ of Ω and we define

- $\mathcal{F}(K)$: the set of the faces of an element K of $\mathcal{T}_h$,
- F one face of K,
- $\mathcal{F}_b$: the set of the boundary faces F_b, i.e. $F_b = \partial K \cap \Gamma$, where $\Gamma = \partial\Omega$,
- $\mathcal{F}_i$: the set of the interior faces F_i i.e. $F_i = \partial K \cap \partial K'$ where K and K' are neighbours,
- $\mathcal{F}_h$: the set of all the faces of the mesh, i.e. $\mathcal{F}_h = \mathcal{F}_i \cup \mathcal{F}_b$,
- $\mathbf{n}$: the outward unit normal vector to K, $\mathbf{t}$ its tangent.

For an interior interface $F = \partial K^+ \cap \partial K^- \in \mathcal{F}_i$ we define the jump $[\![\cdot]\!]$ of a vector $\mathbf{v}$ such as

$$[\![\mathbf{v} \cdot \mathbf{n}]\!] = \mathbf{v}^+ \cdot \mathbf{n}^+ + \mathbf{v}^- \cdot \mathbf{n}^-.$$

For a boundary face $F = \partial K^+ \cap \Gamma \in \mathcal{F}_b$ we define it such as

$$[\![\mathbf{v} \cdot \mathbf{n}]\!] = \mathbf{v}^+ \cdot \mathbf{n}^+.$$

The jump of a tensor $\underline{\underline{\sigma}}$ is defined for an intern face F_i such as

$$[\![\underline{\underline{\sigma}} \cdot \mathbf{n}]\!] = \underline{\underline{\sigma}}^+ \cdot \mathbf{n}^+ + \underline{\underline{\sigma}}^- \cdot \mathbf{n}^-,$$

and on an external face F_b such as

$$[\![\underline{\underline{\sigma}} \cdot \mathbf{n}]\!] = \underline{\underline{\sigma}}^+ \cdot \mathbf{n}^+.$$

We denote $P_p(D)$ the set of polynomials degree at most p on the domain D. For each element $K \in \mathcal{T}_h$, we define $V^p(K)$ as the space $P_p(K)$, $\mathbf{V}^p(K)$ as the space $(P_p(K))^2$ and $\mathbf{\Sigma}^p(K)$ as the space $(P_p(K))^3$. The discontinuous finite element spaces are then given by

$$\begin{aligned}
V_h^p &= \{v \in L^2(\Omega) : \quad v|_K \in V^p(K), \forall K \in \mathcal{T}_h\} \\
\mathbf{V}_h^p &= \{\mathbf{v} \in \left(L^2(\Omega)\right)^2 : \quad \mathbf{v}|_K \in \mathbf{V}^p(K), \forall K \in \mathcal{T}_h\} \\
\mathbf{\Sigma}_h^p &= \{\underline{\underline{\sigma}} \in \left(L^2(\Omega)\right)^3 : \quad \underline{\underline{\sigma}}|_K \in \mathbf{\Sigma}^p(K), \forall K \in \mathcal{T}_h\},
\end{aligned}$$

where $L^2(\Omega)$ is the space of square integrable functions on the domain Ω. Finally we introduce the traced finite element space

$$\mathbf{M}_h = \{\eta \in \left(L^2(\mathcal{F}_h)\right)^2 : \quad \eta|_F \in (P_p(F))^2, \forall F \in \mathcal{F}_h\},$$

where $\mathbf{M}_h$ represents the space of functions that are continuous on an edge but discontinuous at its ends.

3 Hybridizable Discontinuous Galerkin (HDG) method

3.1 HDG formulation

We consider equations (2.1) on an element K of $\mathcal{T}_h$. The *classical* discontinuous Galerkin method seeks an approximate solution $(\mathbf{v}_h, \underline{\underline{\sigma}}_h)$ in the space $\mathbf{V}_h^p \times \mathbf{\Sigma}_h^p$ satisfying for all K in $\mathcal{T}_h$

$$\left\{ \begin{array}{rcl} \displaystyle\int_K i\omega\rho_K \mathbf{v}_h \cdot \mathbf{w} - \int_K \left(\nabla \cdot \underline{\underline{\sigma}}_h\right) \cdot \mathbf{w} & = & \displaystyle\int_K \mathbf{f} \cdot \mathbf{w}, \\ \displaystyle\int_K i\omega \underline{\underline{\sigma}}_h : \underline{\underline{\xi}} - \int_K \left(\underline{\underline{C}}_K \underline{\underline{\epsilon}}(\mathbf{v}_h)\right) : \underline{\underline{\xi}} & = & 0. \end{array} \right. \tag{3.1}$$

We denote by $\underline{\underline{a}} : \underline{\underline{b}}$ the scalar product between two tensors $\underline{\underline{a}}$ and $\underline{\underline{b}}$. Integrating by parts we obtain

$$\left\{ \begin{array}{rcl} \displaystyle\int_K i\omega\rho_K \mathbf{v}_h \cdot \mathbf{w} + \int_K \underline{\underline{\sigma}}_h : \nabla \mathbf{w} - \int_{\partial K} \widehat{\underline{\underline{\sigma}}}_h \cdot \mathbf{n} \cdot \mathbf{w} & = & \displaystyle\int_K \mathbf{f} \cdot \mathbf{w}, \\ \displaystyle\int_K i\omega \underline{\underline{\sigma}}_h : \underline{\underline{\xi}} + \int_K \mathbf{v}_h \cdot \nabla \cdot \left(\underline{\underline{C}}_K \underline{\underline{\xi}}\right) - \int_{\partial K} \widehat{\mathbf{v}}_h \cdot \underline{\underline{C}}_K \underline{\underline{\xi}} \cdot \mathbf{n} & = & 0. \end{array} \right. \tag{3.2}$$

We then replace the boundary terms by the numerical traces $\widehat{\underline{\underline{\sigma}}}_h$ and $\widehat{\mathbf{v}}$ which are respectively the approximations of $\underline{\underline{\sigma}}$ and $\mathbf{v}$ on ∂K. The principle of the HDG formulation is to express $(\mathbf{v}_h, \underline{\underline{\sigma}}_h)$ in terms of a hybrid unknown λ_h only. This unknown $\lambda_h \in \mathbf{M}_h$ is a Lagrange multiplier and is mainly introduced in order to replace the numerical trace $\widehat{\mathbf{v}}$. This is written as

$$\widehat{\mathbf{v}}_h = \lambda_h, \forall F \in \mathcal{F}_h, \qquad \lambda_h \in \mathbf{M}_h^0. \tag{3.3}$$

Then, we define the numerical trace $\widehat{\underline{\underline{\sigma}}}_h$ in terms of the other unknowns through the relation

$$\widehat{\underline{\underline{\sigma}}}_h = \underline{\underline{\sigma}}_h - \mathbf{S}\left(\mathbf{v}_h - \lambda_h\right) \otimes \mathbf{n} \qquad \text{on } \partial K. \tag{3.4}$$

The matrix $\mathbf{S}$ is a local stabilization matrix which has an important effect on both accuracy and stability of the HDG scheme. Note that we have deduced the numerical trace (3.4) from the one adopted in [3] where the authors consider the displacement gradient-velocity-pressure formulation of the elastodynamics equations, and define

$$\mu \widehat{\mathbf{H}}_h^n + \widehat{p}_h^n \mathbf{I} = \mu \mathbf{H}_h^n + p_h^n \mathbf{I} - \mathbf{S}\left(\mathbf{v}_h - \widehat{\mathbf{v}}_h\right) \otimes \mathbf{n}, \tag{3.5}$$

where $\mathbf{H} = \nabla \mathbf{u}$ is the displacement gradient tensor and $p = (\mu + \lambda)(\nabla \cdot \mathbf{u})$ is the hydrostatic pressure. We have

$$\nabla\left(\mu \mathbf{H}_h^n + p_h^n \mathbf{I}\right) = \nabla \underline{\underline{\sigma}}. \tag{3.6}$$

Assuming that

$$\nabla\left(\mu \widehat{\mathbf{H}}_h^n + \widehat{p}_h^n \mathbf{I}\right) = \nabla \widehat{\underline{\underline{\sigma}}}, \tag{3.7}$$

and replacing $\left(\mu \widehat{\mathbf{H}}_h^n + \widehat{p}_h^n \mathbf{I}\right)$ in this equation by its definition giving by (3.5), we found that

$$\nabla \widehat{\underline{\underline{\sigma}}} = \nabla\left(\underline{\underline{\sigma}} - \mathbf{S}\left(\mathbf{v}_h - \widehat{\mathbf{v}}_h\right) \otimes \mathbf{n}\right), \tag{3.8}$$

and so the definition (3.4). Moreover, in [3], it is proved from the energy identity that $\mathbf{S}$ should have the form $\tau \mathbf{I}$ where $\tau > 0$ is a local stabilization parameter and $\mathbf{I}$ the identity matrix.

By summing (3.2) over all elements and enforcing the continuity of the normal component of $\widehat{\underline{\underline{\sigma}}}_h$, the problem can be rewritten in the following way: find $(\mathbf{v}_h, \underline{\underline{\sigma}}_h, \lambda_h) \in \mathbf{V}_h^p \times \mathbf{\Sigma}_h^p \times \mathbf{M}_h$ such that $\forall (\mathbf{w}, \underline{\underline{\xi}}, \eta) \in \mathbf{V}^p(K) \times \mathbf{\Sigma}^p(K) \times \mathbf{M}_h$

$$\left\{\begin{array}{rcl} \displaystyle\sum_{K\in\mathcal{T}_h}\int_K i\omega\rho_K\mathbf{v}_h\cdot\mathbf{w} + \sum_{K\in\mathcal{T}_h}\int_K \underline{\underline{\sigma}}_h : \nabla\mathbf{w} - \sum_{K\in\mathcal{T}_h}\int_{\partial K}\widehat{\underline{\underline{\sigma}}}_h\cdot\mathbf{n}\cdot\mathbf{w} &=& \displaystyle\sum_{K\in\mathcal{T}_h}\int_K \mathbf{f}\cdot\mathbf{w}, \\ \displaystyle\sum_{K\in\mathcal{T}_h}\int_K i\omega\underline{\underline{\sigma}}_h : \underline{\underline{\xi}} + \sum_{K\in\mathcal{T}_h}\int_K \mathbf{v}_h\cdot\nabla\cdot\left(\underline{\underline{C}}_K\underline{\underline{\xi}}\right) - \sum_{K\in\mathcal{T}_h}\int_{\partial K}\lambda_h\cdot\underline{\underline{C}}_K\underline{\underline{\xi}}\cdot\mathbf{n} &=& 0, \\ \displaystyle\sum_{F\in\mathcal{F}_h}\int_F [\![\widehat{\underline{\underline{\sigma}}}_h\cdot\mathbf{n}]\!]\cdot\eta &=& 0. \end{array}\right. \tag{3.9}$$

We remark that the continuity of the normal component of $\widehat{\underline{\underline{\sigma}}}_h$ is imposed by the last equation of (3.9) which is called the *conservativity condition*. According to (3.4), we note that on ∂K

$$\widehat{\underline{\underline{\sigma}}}_h\cdot\mathbf{n} = \underline{\underline{\sigma}}_h\cdot\mathbf{n} - \mathbf{S}\left(\mathbf{v}_h - \widehat{\mathbf{v}}_h\right). \tag{3.10}$$

It is clear that for a face $F = \partial K^+ \cap \partial K^-$

$$\begin{aligned} \int_F [\![\widehat{\underline{\underline{\sigma}}}_h\cdot\mathbf{n}]\!]\cdot\eta &= \int_F [\![\underline{\underline{\sigma}}_h\cdot\mathbf{n} - \mathbf{S}\left(\mathbf{v}_h - \widehat{\mathbf{v}}_h\right)]\!]\cdot\eta \\ &= \int_F \left(\underline{\underline{\sigma}}_h^{K^+}\cdot\mathbf{n}^{K^+} - \mathbf{S}^{K^+}\left(\mathbf{v}_h^{K^+} - \widehat{\mathbf{v}}_h\right)\right)\cdot\eta \\ &+ \int_F \left(\underline{\underline{\sigma}}_h^{K^-}\cdot\mathbf{n}^{K^-} - \mathbf{S}^{K^-}\left(\mathbf{v}_h^{K^-} - \widehat{\mathbf{v}}_h\right)\right)\cdot\eta, \end{aligned}$$

thus

$$\sum_{F\in\mathcal{F}_h}\int_F [\![\widehat{\underline{\underline{\sigma}}}_h\cdot\mathbf{n}]\!]\cdot\eta = \sum_{K\in\mathcal{T}_h}\int_{\partial K}\left(\underline{\underline{\sigma}}_h\cdot\mathbf{n}\right)\cdot\eta - \sum_{K\in\mathcal{T}_h}\int_{\partial K}\mathbf{S}\left(\mathbf{v}_h - \widehat{\mathbf{v}}_h\right)\cdot\eta.$$

In order to obtain the global HDG formulation, we rewrite system (3.9) as

$$\left\{\begin{array}{rcl} \displaystyle\sum_{K\in\mathcal{T}_h}\int_K i\omega\rho_K\mathbf{v}_h\cdot\mathbf{w} - \sum_{K\in\mathcal{T}_h}\int_K\left(\nabla\cdot\underline{\underline{\sigma}}_h\right)\cdot\mathbf{w} & & \\ \qquad + \displaystyle\sum_{K\in\mathcal{T}_h}\int_{\partial K}\mathbf{S}\left(\mathbf{v}_h - \lambda_h\right)\cdot\mathbf{w} &=& \displaystyle\sum_{K\in\mathcal{T}_h}\int_K\mathbf{f}\cdot\mathbf{w}, \\ \displaystyle\sum_{K\in\mathcal{T}_h}\int_K i\omega\underline{\underline{\sigma}}_h : \underline{\underline{\xi}} + \sum_{K\in\mathcal{T}_h}\int_K \mathbf{v}_h\cdot\nabla\cdot\left(\underline{\underline{C}}_K\underline{\underline{\xi}}\right) - \sum_{K\in\mathcal{T}_h}\int_{\partial K}\lambda_h\cdot\underline{\underline{C}}_K\underline{\underline{\xi}}\cdot\mathbf{n} &=& 0, \\ \displaystyle\sum_{K\in\mathcal{T}_h}\int_{\partial K}\left(\underline{\underline{\sigma}}_h\cdot\mathbf{n}\right)\cdot\eta - \sum_{K\in\mathcal{T}_h}\int_{\partial K}\mathbf{S}\left(\mathbf{v}_h - \lambda_h\right)\cdot\eta &=& 0. \end{array}\right. \tag{3.11}$$

The local problem on an element K is then written as

$$\left\{\begin{array}{rcl} \displaystyle\int_K i\omega\rho_K\mathbf{v}_h^K\cdot\mathbf{w} - \int_K\left(\nabla\cdot\underline{\underline{\sigma}}_h^K\right)\cdot\mathbf{w} + \int_{\partial K}\mathbf{S}\left(\mathbf{v}_h^K - \lambda_h\right)\cdot\mathbf{w} &=& \displaystyle\int_K\mathbf{f}^K\cdot w, \\ \displaystyle\int_K i\omega\underline{\underline{\sigma}}_h^K : \underline{\underline{\xi}} + \int_K\mathbf{v}_h^K\cdot\nabla\cdot\left(\underline{\underline{C}}_K\underline{\underline{\xi}}\right) - \int_{\partial K}\lambda_h\cdot\underline{\underline{C}}_K\underline{\underline{\xi}}\cdot\mathbf{n} &=& 0. \end{array}\right. \tag{3.12}$$

3.2 Relationship between HDG and upwind flux DG

The conservativity condition is given by

$$\sum_{F\in\mathcal{F}_i}\int_F [\![\widehat{\underline{\underline{\sigma}}}_h\cdot\mathbf{n}]\!]\cdot\eta=0\quad\forall\eta\in\mathbf{M}_h.$$

Considering interpolation spaces with p constant, we can deduce that

$$[\![\widehat{\underline{\underline{\sigma}}}_h\cdot\mathbf{n}]\!]=0\quad\forall F\in\mathcal{F}_i.$$

Substituing $\widehat{\underline{\underline{\sigma}}}_h$ by the expression (3.4) and assuming $\mathbf{S}^+ + \mathbf{S}^- \neq 0$, where $\mathbf{S}^+$ is the stabilization matrix on the element K^+ and $\mathbf{S}^-$ the stabilization matrix on K^-, we obtain

$$[\![\underline{\underline{\sigma}}_h\cdot\mathbf{n}-\mathbf{S}\left(\mathbf{v}_h-\lambda_h\right)]\!]=[\![\underline{\underline{\sigma}}_h\cdot\mathbf{n}]\!]-\left(\mathbf{S}^+\mathbf{v}_h^+ + \mathbf{S}^-\mathbf{v}_h^-\right)+\lambda_h\left(\mathbf{S}^+ + \mathbf{S}^-\right).$$

Solving for λ_h, we get

$$\widehat{\mathbf{v}}_h=\lambda_h=\left(\mathbf{S}^+ + \mathbf{S}^-\right)^{-1}\left(\mathbf{S}^+\mathbf{v}_h^+ + \mathbf{S}^-\mathbf{v}_h^-\right)-\left(\mathbf{S}^+ + \mathbf{S}^-\right)^{-1}[\![\underline{\underline{\sigma}}_h\cdot\mathbf{n}]\!].\tag{3.13}$$

Inserting this expression for λ_h into the following expression

$$\widehat{\underline{\underline{\sigma}}}_h^{\pm}\cdot\mathbf{n}^{\pm}=\underline{\underline{\sigma}}_h^{\pm}\cdot\mathbf{n}^{\pm}+\left(\mathbf{S}^{\pm}\left(\mathbf{v}_h^{\pm}-\lambda_h\right)\right)\cdot\mathbf{n}^{\pm},\tag{3.14}$$

we finally obtain

$$\widehat{\underline{\underline{\sigma}}}_h^{\pm}\cdot\mathbf{n}^{\pm}=\widetilde{\underline{\underline{\sigma}}}_h\cdot\mathbf{n}^{\pm},$$

where

$$\widetilde{\underline{\underline{\sigma}}}_h=\mathbf{S}^-\left(\mathbf{S}^+ + \mathbf{S}^-\right)^{-1}\underline{\underline{\sigma}}_h^+ + \mathbf{S}^+\left(\mathbf{S}^+ + \mathbf{S}^-\right)^{-1}\underline{\underline{\sigma}}_h^- - \mathbf{S}^+\left(\mathbf{S}^+ + \mathbf{S}^-\right)^{-1}\mathbf{S}^-[\![\mathbf{v}_h\otimes\mathbf{n}]\!].$$

Considering $\mathbf{S}=\tau\mathbf{I}$, we rewrite equation (3.13) and $\widetilde{\underline{\underline{\sigma}}}_h$ as

$$\lambda_h=\frac{1}{(\tau^+ + \tau^-)}\mathbf{I}\left(\tau^+\mathbf{v}_h^+ + \tau^-\mathbf{v}_h^-\right)-\frac{1}{(\tau^+ + \tau^-)}\mathbf{I}[\![\underline{\underline{\sigma}}_h\cdot\mathbf{n}]\!],$$

$$\widetilde{\underline{\underline{\sigma}}}_h=\frac{1}{(\tau^+ + \tau^-)}\mathbf{I}\left(\tau^-\underline{\underline{\sigma}}_h^+ + \tau^+\underline{\underline{\sigma}}_h^-\right)-\frac{\tau^+\tau^-}{(\tau^+ + \tau^-)}\mathbf{I}[\![\mathbf{v}_h\otimes\mathbf{n}]\!].$$

3.3 Well-posedness of the local problems

We consider the local equations (3.12) with no source term

$$\begin{cases}\displaystyle\int_K i\omega\rho_K\mathbf{v}_h^K\cdot\mathbf{w}-\int_K\left(\nabla\cdot\underline{\underline{\sigma}}_h^K\right)\cdot\mathbf{w}+\int_{\partial K}\mathbf{S}\left(\mathbf{v}_h^K-\lambda_h\right)\cdot\mathbf{w}=0,\qquad\forall\mathbf{w}\in\mathbf{V}^p(K),\\ \displaystyle\int_K i\omega\underline{\underline{\sigma}}_h^K:\underline{\underline{\xi}}+\int_K\mathbf{v}_h^K\cdot\nabla\cdot\left(\underline{\underline{C}}_K\underline{\underline{\xi}}\right)-\int_{\partial K}\lambda_h\cdot\underline{\underline{C}}_K\underline{\underline{\xi}}\cdot\mathbf{n}=0,\qquad\forall\xi\in\mathbf{\Sigma}^p(K).\end{cases}\tag{3.15}$$

We choose $\mathbf{w}=\overline{\mathbf{v}}_h^K$ and $\xi=\underline{\underline{\mathbf{C}}}^{K^{-1}}\overline{\underline{\underline{\sigma}}}_h^K$ as test functions and we add the two above equations. We obtain

$$\int_K i\omega\rho_K\mathbf{v}_h^K\cdot\overline{\mathbf{v}}_h^K-\int_K\left(\nabla\cdot\underline{\underline{\sigma}}_h^K\right)\cdot\overline{\mathbf{v}}_h^K+\int_{\partial K}\mathbf{S}\left(\mathbf{v}_h^K-\lambda_h\right)\cdot\overline{\mathbf{v}}_h^K+$$
$$\int_K i\omega\underline{\underline{\sigma}}_h^K:\underline{\underline{\mathbf{C}}}^{-1}\overline{\underline{\underline{\sigma}}}_h^K+\int_K\mathbf{v}_h^K\cdot\nabla\cdot\left(\overline{\underline{\underline{\sigma}}}_h^K\right)-\int_{\partial K}\lambda_h\cdot\overline{\underline{\underline{\sigma}}}_h^K\cdot\mathbf{n}=0.$$

Setting $\lambda_h = 0$, we get

$$\int_K i\omega\rho_K \mathbf{v}_h^K \cdot \overline{\mathbf{v}}_h^K + \int_K i\omega \underline{\underline{\mathbf{C}}}^{-1} \underline{\underline{\sigma}}_h^K : \overline{\underline{\underline{\sigma}}}_h^K + 2\Im\left(\left(\nabla \cdot \underline{\underline{\sigma}}_h^K\right) \cdot \overline{\mathbf{v}}_h^K\right) + \int_{\partial K} \mathbf{S}\mathbf{v}_h^K \cdot \overline{\mathbf{v}}_h^K = 0. \tag{3.16}$$

Assuming that $\omega, \rho, \underline{\underline{\mathbf{C}}}^{-1}$, and $\mathbf{S}$ are strictly positive real numbers and matrices, if we consider the real part (3.16), we have $\displaystyle\int_{\partial K} \mathbf{S}\mathbf{v}_h^K \cdot \overline{\mathbf{v}}_h^K = 0$ which implies that $\mathbf{v}_h^K = 0$ on ∂K. For the HDG-$\mathbb{P}_1$ formulation, all the degrees of freedom are on ∂K, so $\mathbf{v}_h^K = 0$ on the entire element K.

4 Implementation

4.1 Discretization for the isotropic case

We first consider the isotropic case and we assume that the right-hand side $\mathbf{f}$ is equal to zero. Taking as test function the basis function φ^K, we develop the local equations (3.12) and write the local solution $(\mathbf{v}^K, \underline{\underline{\sigma}}^K)$ as a function of λ (simplified notation for λ_h). In order to avoid confusion with λ the Lamé's coefficient and λ the Lagrange multiplier, we denote by λ_L the Lamé's coefficient.

$$\left\{\begin{array}{rcl}
\displaystyle\int_K i\omega\rho_K v_x^K \varphi^K - \int_K \frac{\partial \sigma_{xx}^K}{\partial x}\varphi^K - \int_K \frac{\partial \sigma_{xz}^K}{\partial z}\varphi^K + \int_{\partial K} \tau^K v_x^K \varphi^K - \int_{\partial K} \tau^K \lambda_x \varphi^K &=& 0,\\
\displaystyle\int_K i\omega\rho_K v_z^K \varphi^K - \int_K \frac{\partial \sigma_{xz}^K}{\partial x}\varphi^K - \int_K \frac{\partial \sigma_{zz}^K}{\partial z}\varphi^K + \int_{\partial K} \tau^K v_z^K \varphi^K - \int_{\partial K} \tau^K \lambda_z \varphi^K &=& 0,\\
\displaystyle\int_K i\omega\sigma_{xx}^K \varphi^K + \int_K (\lambda_L + 2\mu)\, v_x^K \frac{\partial \varphi^K}{\partial x} + \int_K \lambda_L v_z^K \frac{\partial \varphi^K}{\partial z} & & \\
\displaystyle - \int_{\partial K} (\lambda_L + 2\mu)\, \lambda_x \varphi^K n_x - \int_{\partial K} \lambda_L \lambda_z \varphi^K n_z &=& 0,\\
\displaystyle\int_K i\omega\sigma_{zz}^K \varphi^K + \int_K \lambda_L v_x^K \frac{\partial \varphi^K}{\partial x} + \int_K (\lambda_L + 2\mu)\, v_z^K \frac{\partial \varphi^K}{\partial z} & & \\
\displaystyle - \int_{\partial K} \lambda_L \lambda_x \varphi^K n_x - \int_{\partial K} (\lambda_L + 2\mu)\, \lambda_z \varphi^K n_z &=& 0,\\
\displaystyle\int_K i\omega\sigma_{xz}^K \varphi^K + \int_K \mu v_x^K \frac{\partial \varphi^K}{\partial z} + \int_K \mu v_z^K \frac{\partial \varphi^K}{\partial x} - \int_{\partial K} \mu\lambda_x \varphi^K n_z - \int_{\partial K} \mu\lambda_z \varphi^K n_x &=& 0.
\end{array}\right. \tag{4.1}$$

For an element K, we define $\left(\varphi_j^K\right)_{j=1,..,d_i^K}$ the basis functions with d_i^K the number of degrees of freedom. We decompose the local solutions $(\mathbf{v}^K, \underline{\underline{\sigma}}^K)$ on the basis $\left(\varphi_j^K\right)$ as follow

$$\begin{aligned}
v_l^K &= \sum_{j=1}^{d_i^K} \underline{v}_{l,j}^K \varphi_j^K, \qquad l = x, z,\\
\sigma_{kl}^K &= \sum_{j=1}^{d_i^K} \underline{\sigma}_{kl,j}^K \varphi_j^K, \qquad k, l = x, z,
\end{aligned} \tag{4.2}$$

For a face F, λ is represented by

$$\lambda_l^F = \sum_{j=1}^{d_i^F} \underline{\lambda}_{l,j}^F \psi_j^F, \qquad l = x, z, \tag{4.3}$$

where ψ_j^F are the basis functions of $P_p(F)$ and d_i^F the associated degrees of freedom. We denote by $\beta(K,l)$ the global index of the l-th face of the element K ($l=1,2,3$). For example if the l-th face of K is the j-th face F_j then $\beta(K,l)=j$. Similarly, if F_l is the common face between K^e and K^f, we define $\eta(l,+)=e$ and $\eta(l,-)=f$. After discretization, the local linear system resulting from (4.1) writes

$$
\left\{
\begin{array}{rcl}
i\omega\rho\mathbb{M}^K\underline{v}_x^K &-& \mathbb{D}_x^{K^T}\underline{\sigma}_{xx}^K - \mathbb{D}_z^{K^T}\underline{\sigma}_{xz}^K + \displaystyle\sum_{l=1}^{3}\tau^{(K,l)}\mathbb{E}_l^K\underline{v}_x^K \\
&-& \displaystyle\sum_{l=1}^{3}\tau^{(K,l)}\mathbb{F}_l^K\underline{\lambda}_x^{\beta(K,l)} = 0, \\
i\omega\rho\mathbb{M}^K\underline{v}_z^K &-& \mathbb{D}_x^{K^T}\underline{\sigma}_{xz}^K - \mathbb{D}_z^{K^T}\underline{\sigma}_{zz}^K + \displaystyle\sum_{l=1}^{3}\tau^{(K,l)}\mathbb{E}_l^K\underline{v}_z^K \\
&-& \displaystyle\sum_{l=1}^{3}\tau^{(K,l)}\mathbb{F}_l^K\underline{\lambda}_z^{\beta(K,l)} = 0, \\
i\omega\mathbb{M}^K\underline{\sigma}_{xx}^K &+& (\lambda_L+2\mu)\mathbb{D}_x^K\underline{v}_x^K + \lambda_L\mathbb{D}_z^K\underline{v}_z^K - \displaystyle\sum_{l=1}^{3}(\lambda_L+2\mu)\underline{\lambda}_x^{\beta(K,l)}\mathbb{Q}_{xl}^K \\
&-& \displaystyle\sum_{l=1}^{3}\lambda_L\underline{\lambda}_z^{\beta(K,l)}\mathbb{Q}_{zl}^K = 0, \\
i\omega\mathbb{M}^K\underline{\sigma}_{zz}^K &+& (\lambda_L+2\mu)\mathbb{D}_z^K\underline{v}_z^K + \lambda_L\mathbb{D}_x^K\underline{v}_x^K - \displaystyle\sum_{l=1}^{3}(\lambda_L+2\mu)\underline{\lambda}_z^{\beta(K,l)}\mathbb{Q}_{zl}^K \\
&-& \displaystyle\sum_{l=1}^{3}\lambda_L\underline{\lambda}_x^{\beta(K,l)}\mathbb{Q}_{xl}^K = 0, \\
i\omega\mathbb{M}^K\underline{\sigma}_{xz}^K &+& \mu\left(\mathbb{D}_x^K\underline{v}_z^K + \mathbb{D}_z^K\underline{v}_x^K\right) \\
&-& \displaystyle\sum_{l=1}^{3}\mu\left(\underline{\lambda}_x^{\beta(K,l)}\mathbb{Q}_{zl}^K + \underline{\lambda}_z^{\beta(K,l)}\mathbb{Q}_{xl}^K\right) = 0.
\end{array}
\right. \tag{4.4}
$$

The entries of the local matrices are defined by

$$
\left\{
\begin{array}{l}
\mathbb{M}_{ij}^K = \displaystyle\int_K \varphi_i^K\varphi_j^K d\mathbf{x}, \\[2ex]
\mathbb{D}_{u,ij}^K = \displaystyle\int_K \varphi_i^K\partial_u\varphi_j^K d\mathbf{x}, \quad \text{with } u=x,z, \\[2ex]
\mathbb{E}_{l,ij}^K = \displaystyle\int_{\partial K^l} \varphi_i^K\varphi_j^K ds, \\[2ex]
\mathbb{F}_{l,ij}^K = \displaystyle\int_{\partial K^l} \psi_i^{\beta(K,l)}\varphi_j^K ds, \\[2ex]
\mathbb{Q}_{ul,ij}^K = \displaystyle\int_{\partial K^l} n_u^K\psi_i^{\beta(K,l)}\varphi_j^K, \quad \text{with } u=x,z.
\end{array}
\right.
$$

where ∂K^l denotes the face of index l of the element K. From (4.4) we can obtain the unknowns variables $\underline{W}^K = \left(\underline{v}_x^K, \quad \underline{v}_z^K, \quad \underline{\sigma}_{xx}^K, \quad \underline{\sigma}_{zz}^K, \quad \underline{\sigma}_{xz}^K\right)^T$
provided by $\underline{\Lambda}^K = \left(\underline{\lambda}_x^{\beta(K,1)}, \quad \underline{\lambda}_x^{\beta(K,2)}, \quad \underline{\lambda}_x^{\beta(K,3)}, \quad \underline{\lambda}_z^{\beta(K,1)}, \quad \underline{\lambda}_z^{\beta(K,2)}, \quad \underline{\lambda}_z^{\beta(K,3)}\right)^T$. The local linear system on the element K can be written as

$$\mathbb{A}^K \underline{W}^K + \mathbb{C}^K \underline{\Lambda}^K = 0, \tag{4.5}$$

with

$$\mathbb{A}^K = \begin{bmatrix} i\omega\rho\mathbb{M}^K + \sum_{l=1}^3 \tau^{(K,l)}\mathbb{E}_l^K & 0 & -\mathbb{D}_x^{K^T} & 0 & -\mathbb{D}_z^{K^T} \\ 0 & i\omega\rho\mathbb{M}^K + \sum_{l=1}^3 \tau^{(K,l)}\mathbb{E}_l^K & 0 & -\mathbb{D}_z^{K^T} & -\mathbb{D}_x^{K^T} \\ \xi\mathbb{D}_x^K & \lambda_L\mathbb{D}_z^K & i\omega\mathbb{M}^K & 0 & 0 \\ \lambda_L\mathbb{D}_x^K & \xi\mathbb{D}_z^K & 0 & i\omega\mathbb{M}^K & 0 \\ \mu\mathbb{D}_z^K & \mu\mathbb{D}_x^K & 0 & 0 & i\omega\mathbb{M}^K \end{bmatrix},$$

$$\mathbb{C}^K = -\begin{bmatrix} \tau^{(K,1)}\mathbb{F}_1^K & \tau^{(K,2)}\mathbb{F}_2^K & \tau^{(K,3)}\mathbb{F}_3^K & 0 & 0 & 0 \\ 0 & 0 & 0 & \tau^{(K,1)}\mathbb{F}_1^K & \tau^{(K,2)}\mathbb{F}_2^K & \tau^{(K,3)}\mathbb{F}_3^K \\ \xi\mathbb{Q}_{x1}^K & \xi\mathbb{Q}_{x2}^K & \xi\mathbb{Q}_{x3}^K & \lambda_L\mathbb{Q}_{z1}^K & \lambda_L\mathbb{Q}_{z2}^K & \lambda_L\mathbb{Q}_{z3}^K \\ \lambda_L\mathbb{Q}_{x1}^K & \lambda_L\mathbb{Q}_{x2}^K & \lambda_L\mathbb{Q}_{x3}^K & \xi\mathbb{Q}_{z1}^K & \xi\mathbb{Q}_{z2}^K & \xi\mathbb{Q}_{z3}^K \\ \mu\mathbb{Q}_{z1}^K & \mu\mathbb{Q}_{z2}^K & \mu\mathbb{Q}_{z3}^K & \mu\mathbb{Q}_{x1}^K & \mu\mathbb{Q}_{x2}^K & \mu\mathbb{Q}_{x3}^K \end{bmatrix}.$$

with $\xi = \lambda_L + 2\mu$. We consider now the discretization of the transmission condition (the last equation of (3.11)). We remind that the transmission condition on a face $F_j = \partial K^+ \cap \partial K^-$ such as $j = \beta(K^+, l) = \beta(K^-, g)$ is written as, $\forall \eta \in \mathbf{M}_h$

$$\int_F \left(\underline{\underline{\sigma}}_h^{K^+} \cdot \mathbf{n}^{K^+} \cdot \eta + \underline{\underline{\sigma}}_h^{K^-} \cdot \mathbf{n}^{K^-} \cdot \eta - \mathbf{S}^{K^+}\left(\mathbf{v}_h^{K^+} - \lambda_h\right) \cdot \eta - \mathbf{S}^{K^-}\left(\mathbf{v}_h^{K^-} - \lambda_h\right) \cdot \eta\right) = 0.$$

The resulting discretization is given by the two following systems

$$\begin{aligned} &\mathbb{Q}_{xl}^{K^+{}^T}\underline{\sigma}_{xx}^{K^+} + \mathbb{Q}_{zl}^{K^+{}^T}\underline{\sigma}_{xz}^{K^+} - \tau^{(K^+,l)}\mathbb{F}_l^{K^+{}^T}\underline{v}_x^{K^+} + \tau^{(K^+,l)}\mathbb{G}^j\underline{\lambda}_x^{\beta(K^+,l)} + \\ &\mathbb{Q}_{xl}^{K^-{}^T}\underline{\sigma}_{xx}^{K^-} + \mathbb{Q}_{zl}^{K^-{}^T}\underline{\sigma}_{xz}^{K^-} - \tau^{(K^-,l)}\mathbb{F}_l^{K^-{}^T}\underline{v}_x^{K^-} + \tau^{(K^-,l)}\mathbb{G}^j\underline{\lambda}_x^{\beta(K^-,l)} = 0, \end{aligned} \tag{4.6}$$

and

$$\begin{aligned} &\mathbb{Q}_{xl}^{K^+{}^T}\underline{\sigma}_{xz}^{K^+} + \mathbb{Q}_{zl}^{K^+{}^T}\underline{\sigma}_{zz}^{K^+} - \tau^{(K^+,l)}\mathbb{F}_l^{K^+{}^T}\underline{v}_z^{K^+} + \tau^{(K^+,l)}\mathbb{G}^j\underline{\lambda}_z^{\beta(K^+,l)} + \\ &\mathbb{Q}_{xl}^{K^-{}^T}\underline{\sigma}_{xz}^{K^-} + \mathbb{Q}_{zl}^{K^-{}^T}\underline{\sigma}_{xz}^{K^-} - \tau^{(K^-,l)}\mathbb{F}_l^{K^-{}^T}\underline{v}_z^{K^-} + \tau^{(K^-,l)}\mathbb{G}^j\underline{\lambda}_z^{\beta(K^-,l)} = 0, \end{aligned} \tag{4.7}$$

where

$$\mathbb{G}_{im}^j = \int_{F_j} \psi_i \psi_m ds.$$

From (4.6) and (4.7) we can write a local system for λ

$$\mathbb{B}^K \underline{W}^K + \mathbb{L}^K \underline{\Lambda}^K + \mathcal{R}^K = 0, \tag{4.8}$$

with

$$\mathbb{B}^K = \begin{bmatrix} -\tau^{(K,1)}\mathbb{F}_1^{K^T} & 0 & \mathbb{Q}_{x1}^{K^T} & 0 & \mathbb{Q}_{z1}^{K^T} \\ -\tau^{(K,2)}\mathbb{F}_2^{K} & 0 & \mathbb{Q}_{x2}^{K^T} & 0 & \mathbb{Q}_{z2}^{K^T} \\ -\tau^{(K,3)}\mathbb{F}_3^{K^T} & 0 & \mathbb{Q}_{x3}^{K^T} & 0 & \mathbb{Q}_{z3}^{K^T} \\ 0 & -\tau^{(K,1)}\mathbb{F}_1^{K^T} & 0 & \mathbb{Q}_{z1}^{K^T} & \mathbb{Q}_{x1}^{K^T} \\ 0 & -\tau^{(K,2)}\mathbb{F}_2^{K^T} & 0 & \mathbb{Q}_{z2}^{K^T} & \mathbb{Q}_{x2}^{K^T} \\ 0 & -\tau^{(K,3)}\mathbb{F}_3^{K^T} & 0 & \mathbb{Q}_{z3}^{K^T} & \mathbb{Q}_{x3}^{K^T} \end{bmatrix},$$

$$\mathbb{L}^K = \begin{bmatrix} \tau^{(K,1)}\mathbb{G}^{\beta(K,1)} & 0 & 0 & 0 & 0 & 0 \\ 0 & \tau^{(K,2)}\mathbb{G}^{\beta(K,2)} & 0 & 0 & 0 & 0 \\ 0 & 0 & \tau^{(K,3)}\mathbb{G}^{\beta(K,3)} & 0 & 0 & 0 \\ 0 & 0 & 0 & \tau^{(K,1)}\mathbb{G}^{\beta(K,1)} & 0 & 0 \\ 0 & 0 & 0 & 0 & \tau^{(K,2)}\mathbb{G}^{\beta(K,2)} & 0 \\ 0 & 0 & 0 & 0 & 0 & \tau^{(K,3)}\mathbb{G}^{\beta(K,3)} \end{bmatrix},$$

and $\mathcal{R}^K$ gathers the contributions from the neighboring elements. We denote by $N_\lambda^{(e,l)}$ the number of degrees of freedom (dof) of the l-th face of K_e, N_λ the total number of dof of Λ and

$$\overline{N}_\lambda = \sum_{e=1}^{N_e} \sum_{l=1}^{3} N^{(e,l)}.$$

We define the trace space spreading operator $\mathcal{A}_{HDG}$ as a matrix of size $\overline{N}_\lambda \times N_\lambda$ which allows to map the unique global trace space values $\underline{\Lambda}$ onto their local values on each face of the element K, $\underline{\Lambda}^K$. We can organize $\mathcal{A}_{HDG}$ by elements such as

$$\mathcal{A}_{HDG} = \begin{pmatrix} \mathcal{A}_{HDG}^1 \\ \vdots \\ \mathcal{A}_{HDG}^{N_e} \end{pmatrix} \text{ and } \mathcal{A}_{HDG}^K \underline{\Lambda} = \underline{\Lambda}^K.$$

Then we rewrite (4.5) such as

$$\mathbb{A}^K \underline{W}^K + \mathbb{C}^K \mathcal{A}_{HDG}^K \underline{\Lambda} = 0, \tag{4.9}$$

and consequently we can express $\underline{W}^K$ in terms of $\underline{\Lambda}$

$$\underline{W}^K = -(\mathbb{A}^K)^{-1} \mathbb{C}^K \mathcal{A}_{HDG}^K \underline{\Lambda}. \tag{4.10}$$

By summing all the equations of the transmission condition on all the faces of each element, element by element, we obtain

$$\sum_{K\in\mathcal{T}_h} (\mathcal{A}_{HDG}^K)^T \left[\mathbb{B}^K \underline{W}^K + \mathbb{L}^K \mathcal{A}_{HDG}^K \underline{\Lambda}\right] = 0, \tag{4.11}$$

where the sum over all the elements along with the left application of the transpose of $\mathcal{A}_{HDG}^K$ allow to gather the element-wise contributions corresponding to faces. By remplacing $\underline{W}^K$ in (4.11), we obtain a global system in $\underline{\Lambda}$

$$\sum_{K\in\mathcal{T}_h} (\mathcal{A}_{HDG}^K)^T \left[-\mathbb{B}^K (\mathbb{A}^K)^{-1} \mathbb{C}^K + \mathbb{L}^K\right] \mathcal{A}_{HDG}^K \underline{\Lambda} = 0. \tag{4.12}$$

Considering now a nonzero source term, (4.9) becomes

$$\mathbb{A}^K \underline{W}^K + \mathbb{C}^K \mathcal{A}_{HDG}^K \underline{\Lambda} = \mathbb{S}^K.$$

That leads to

$$\underline{W}^K = \left(\mathbb{A}^K\right)^{-1} \mathbb{S}^K - \left(\mathbb{A}^K\right)^{-1} \mathbb{C}^K \mathcal{A}_{HDG}^K \underline{\Lambda}.$$

Finally we obtain the following global system

$$\sum_{K\in\mathcal{T}_h} (\mathcal{A}_{HDG}^K)^T \left[-\mathbb{B}^K (\mathbb{A}^K)^{-1} \mathbb{C}^K + \mathbb{L}^K\right] \mathcal{A}_{HDG}^K \underline{\Lambda} = \sum_{K\in\mathcal{T}_h} -(\mathcal{A}_{HDG}^K)^T \mathbb{B}^K (\mathbb{A}^K)^{-1} \mathbb{S}^K. \tag{4.13}$$

4.2 Discretization for the anisotropic case

Taking the basis function φ_j^K as test function and developing the local equations (3.12) for the anisotropic case as we have done in the previous section, we write the local solution $(\mathbf{v}^K, \underline{\underline{\sigma}}^K)$

as a function of λ

(4.14)

$$
\left\{
\begin{aligned}
&\int_K i\omega\rho_K v_x^K \varphi_j^K - \int_K \frac{\partial \sigma_{xx}^K}{\partial x}\varphi_j^K - \int_K \frac{\partial \sigma_{xz}^K}{\partial z}\varphi_j^K + \int_{\partial K} \tau^K v_x^K \varphi_j^K \\
&\qquad - \int_{\partial K} \tau^K \lambda_x \varphi_j^K = 0, \\
&\int_K i\omega\rho_K v_z^K \varphi_j^K - \int_K \frac{\partial \sigma_{xz}^K}{\partial x}\varphi_j^K - \int_K \frac{\partial \sigma_{zz}^K}{\partial z}\varphi_j^K + \int_{\partial K} \tau^K v_z^K \varphi_j^K \\
&\qquad - \int_{\partial K} \tau^K \lambda_z \varphi_j^K = 0, \\
&\int_K i\omega\sigma_{xx}^K \varphi_j^K + \int_K C_{11} v_x^K \frac{\partial \varphi_j^K}{\partial x} + \int_K C_{12} v_z^K \frac{\partial \varphi_j^K}{\partial z} + \int_K C_{13}\left(v_x^K \frac{\partial \varphi_j^K}{\partial z} + v_z^K \frac{\partial \varphi_j^K}{\partial x}\right) \\
&\qquad - \int_{\partial K} C_{11}\lambda_x \varphi_j^K n_x - \int_{\partial K} C_{12}\lambda_z \varphi_j^K n_z - \int_{\partial K} C_{13}\left(\lambda_x \varphi_j^K n_z + \lambda_z \varphi_j^K n_x\right) = 0, \\
&\int_K i\omega\sigma_{zz}^K \varphi_j^K + \int_K C_{12} v_x^K \frac{\partial \varphi_j^K}{\partial x} + \int_K C_{22} v_z^K \frac{\partial \varphi_j^K}{\partial z} + \int_K C_{23}\left(v_x^K \frac{\partial \varphi_j^K}{\partial z} + v_z^K \frac{\partial \varphi_j^K}{\partial x}\right) \\
&\qquad - \int_{\partial K} C_{12}\lambda_x \varphi_j^K n_x - \int_{\partial K} C_{22}\lambda_z \varphi_j^K n_z - \int_{\partial K} C_{23}\left(\lambda_x \varphi_j^K n_z + \lambda_z \varphi_j^K n_x\right) = 0, \\
&\int_K i\omega\sigma_{xz}^K \varphi_j^K + \int_K C_{13} v_x^K \frac{\partial \varphi_j^K}{\partial x} + \int_K C_{23} v_z^K \frac{\partial \varphi_j^K}{\partial z} + \int_K C_{33}\left(v_x^K \frac{\partial \varphi_j^K}{\partial z} + v_z^K \frac{\partial \varphi_j^K}{\partial x}\right) \\
&\qquad - \int_{\partial K} C_{13}\lambda_x \varphi_j^K n_x - \int_{\partial K} C_{23}\lambda_z \varphi_j^K n_z - \int_{\partial K} C_{33}\left(\lambda_x \varphi_j^K n_z - \lambda_z \varphi_j^K n_x\right) = 0.
\end{aligned}
\right.
$$

Using the discretization given in section 4.1, the local linear system resulting from (4.14) writes as

$$
\left\{
\begin{array}{lcl}
i\omega\rho\mathbb{M}^K\underline{v}_x^K & - & \mathbb{D}_x^{K^T}\underline{\sigma}_{xx}^K - \mathbb{D}_z^{K^T}\underline{\sigma}_{xz}^K \\
& + & \displaystyle\sum_{l=1}^{3}\tau^{(K,l)}\mathbb{E}_l^K\underline{v}_x^K - \sum_{l=1}^{3}\tau^{(K,l)}\mathbb{F}_l^K\underline{\lambda}_x^{\beta(K,l)} = 0 \\
i\omega\rho\mathbb{M}^K\underline{v}_z^K & - & \mathbb{D}_x^{K^T}\underline{\sigma}_{xz}^K - \mathbb{D}_z^{K^T}\underline{\sigma}_{zz}^K \\
& + & \displaystyle\sum_{l=1}^{3}\tau^{(K,l)}\mathbb{E}_l^K\underline{v}_z^K - \sum_{l=1}^{3}\tau^{(K,l)}\mathbb{F}_l^K\underline{\lambda}_z^{\beta(K,l)} = 0 \\
i\omega\mathbb{M}^K\underline{\sigma}_{xx}^K & + & C_{11}^K\mathbb{D}_x^K\underline{v}_x^K + C_{12}^K\mathbb{D}_z^K\underline{v}_z^K \\
& + & C_{13}^K\left(\mathbb{D}_x^K\underline{v}_z^K + \mathbb{D}_z^K\underline{v}_x^K\right) \\
& - & \displaystyle\sum_{l=1}^{3}C_{11}^K\underline{\lambda}_x^{\beta(K,l)}\mathbb{Q}_{xl}^K - \sum_{l=1}^{3}C_{12}^K\underline{\lambda}_z^{\beta(K,l)}\mathbb{Q}_{zl}^K \\
& - & \displaystyle\sum_{l=1}^{3}C_{13}^K\left(\underline{\lambda}_x^{\beta(K,l)}\mathbb{Q}_{zl}^K + \underline{\lambda}_z^{\beta(K,l)}\mathbb{Q}_{xl}^K\right) = 0 \\
i\omega\mathbb{M}^K\underline{\sigma}_{zz}^K & + & C_{12}^K\mathbb{D}_x^K\underline{v}_x^K + C_{22}^K\mathbb{D}_z^K\underline{v}_z^K \\
& + & C_{23}^K\left(\mathbb{D}_x^K\underline{v}_z^K + \mathbb{D}_z^K\underline{v}_x^K\right) \\
& - & \displaystyle\sum_{l=1}^{3}C_{12}^K\underline{\lambda}_x^{\beta(K,l)}\mathbb{Q}_{xl}^K - \sum_{l=1}^{3}C_{22}^K\underline{\lambda}_z^{\beta(K,l)}\mathbb{Q}_{zl}^K \\
& - & \displaystyle\sum_{l=1}^{3}C_{23}^K\left(\underline{\lambda}_x^{\beta(K,l)}\mathbb{Q}_{zl}^K + \underline{\lambda}_z^{\beta(K,l)}\mathbb{Q}_{xl}^K\right) = 0 \\
i\omega\mathbb{M}^K\underline{\sigma}_{xz}^K & + & C_{13}^K\mathbb{D}_x^K\underline{v}_x^K + C_{23}^K\mathbb{D}_z^K\underline{v}_z^K \\
& + & C_{33}^K\left(\mathbb{D}_x^K\underline{v}_z^K + \mathbb{D}_z^K\underline{v}_x^K\right) \\
& - & \displaystyle\sum_{l=1}^{3}C_{13}^K\underline{\lambda}_x^{\beta(K,l)}\mathbb{Q}_{xl}^K - \sum_{l=1}^{3}C_{23}^K\underline{\lambda}_z^{\beta(K,l)}\mathbb{Q}_{zl}^K \\
& - & \displaystyle\sum_{l=1}^{3}C_{33}^K\left(\underline{\lambda}_x^{\beta(K,l)}\mathbb{Q}_{zl}^K + \underline{\lambda}_z^{\beta(K,l)}\mathbb{Q}_{xl}^K\right) = 0,
\end{array}
\right. \tag{4.15}
$$

with matrices $\mathbb{M}^K, \mathbb{D}^K, \mathbb{E}^K, \mathbb{F}^K$ and $\mathbb{Q}^K$ defined in section 4.1. The local linear system on element K is written as in the isotropic case

$$
\mathbb{A}^K\underline{W}^K + \mathbb{C}^K\underline{\Lambda}^K = 0, \tag{4.16}
$$

with

$$
\underline{W}^K = \begin{bmatrix} \underline{v}_x^K \\ \underline{v}_z^K \\ \underline{\sigma}_{xx}^K \\ \underline{\sigma}_{zz}^K \\ \underline{\sigma}_{xz}^K \end{bmatrix}, \qquad \underline{\Lambda}^K = \begin{bmatrix} \underline{\lambda}_x^{\beta(K,1)} \\ \underline{\lambda}_x^{\beta(K,2)} \\ \underline{\lambda}_x^{\beta(K,3)} \\ \underline{\lambda}_z^{\beta(K,1)} \\ \underline{\lambda}_z^{\beta(K,2)} \\ \underline{\lambda}_z^{\beta(K,3)} \end{bmatrix}.
$$

Matrices $\mathbb{A}^K$ and $\mathbb{C}^K$ are now given by

$$\mathbb{A}^K = \begin{bmatrix} i\omega\rho\mathbb{M}^K + \sum_{l=1}^{3}\tau^{(K,l)}\mathbb{E}_l^K & 0 & -\mathbb{D}_x^{K^T} & 0 & -\mathbb{D}_z^{K^T} \\ 0 & i\omega\rho\mathbb{M}^K + \sum_{l=1}^{3}\tau^{(K,l)}\mathbb{E}_l^K & 0 & -\mathbb{D}_z^{K^T} & -\mathbb{D}_x^{K^T} \\ C_{11}^K\mathbb{D}_x^K + C_{13}^K\mathbb{D}_z^K & C_{12}^K\mathbb{D}_z^K + C_{13}^K\mathbb{D}_x^K & i\omega\mathbb{M}^K & 0 & 0 \\ C_{12}^K\mathbb{D}_x^K + C_{23}^K\mathbb{D}_z^K & C_{22}^K\mathbb{D}_z^K + C_{23}^K\mathbb{D}_x^K & 0 & i\omega\mathbb{M}^K & 0 \\ C_{13}^K\mathbb{D}_x^K + C_{33}^K\mathbb{D}_z^K & C_{23}^K\mathbb{D}_z^K + C_{33}^K\mathbb{D}_x^K & 0 & 0 & i\omega\mathbb{M}^K \end{bmatrix},$$

$$\mathbb{C}^K = -\begin{bmatrix} \tau^{(K,1)}\mathbb{F}_1^K & \tau^{(K,2)}\mathbb{F}_2^K & \tau^{(K,3)}\mathbb{F}_3^K & \dots \\ 0 & 0 & 0 & \dots \\ C_{11}^K\mathbb{Q}_{x1}^K + C_{13}^K\mathbb{Q}_{z1}^K & C_{11}^K\mathbb{Q}_{x2}^K + C_{13}^K\mathbb{Q}_{z2}^K & C_{11}^K\mathbb{Q}_{x3}^K + C_{13}^K\mathbb{Q}_{z3}^K & \dots \\ C_{12}^K\mathbb{Q}_{x1}^K + C_{23}^K\mathbb{Q}_{z1}^K & C_{12}^K\mathbb{Q}_{x2}^K + C_{23}^K\mathbb{Q}_{z2}^K & C_{12}^K\mathbb{Q}_{x3}^K + C_{23}^K\mathbb{Q}_{z3}^K & \dots \\ C_{13}^K\mathbb{Q}_{x1}^K + C_{33}^K\mathbb{Q}_{z1}^K & C_{13}^K\mathbb{Q}_{x2}^K + C_{33}^K\mathbb{Q}_{z2}^K & C_{13}^K\mathbb{Q}_{x3}^K + C_{33}^K\mathbb{Q}_{z3}^K & \dots \end{bmatrix}$$
$$\begin{bmatrix} \dots & 0 & 0 & 0 \\ \dots & \tau^{(K,1)}\mathbb{F}_1^K & \tau^{(K,2)}\mathbb{F}_2^K & \tau^{(K,3)}\mathbb{F}_3^K \\ \dots & C_{12}^K\mathbb{Q}_{z1}^K + C_{13}^K\mathbb{Q}_{x1}^K & C_{12}^K\mathbb{Q}_{z2}^K + C_{13}^K\mathbb{Q}_{x2}^K & C_{12}^K\mathbb{Q}_{z3}^K + C_{13}^K\mathbb{Q}_{x3}^K \\ \dots & C_{22}^K\mathbb{Q}_{z1}^K + C_{23}^K\mathbb{Q}_{x1}^K & C_{22}^K\mathbb{Q}_{z2}^K + C_{23}^K\mathbb{Q}_{x2}^K & C_{22}^K\mathbb{Q}_{z3}^K + C_{23}^K\mathbb{Q}_{x3}^K \\ \dots & C_{23}^K\mathbb{Q}_{z1}^K + C_{33}^K\mathbb{Q}_{x1}^K & C_{23}^K\mathbb{Q}_{z2}^K + C_{33}^K\mathbb{Q}_{x2}^K & C_{23}^K\mathbb{Q}_{z3}^K + C_{33}^K\mathbb{Q}_{x3}^K \end{bmatrix}.$$

The transmission condition on a face $F_j = \partial K^+ \cap \partial K^-$ is unchanged and its local discretization reads as

$$\mathbb{B}^K\underline{W}^K + \mathbb{L}^K\underline{\Lambda}^K + \mathcal{R}^K = 0.$$

The matrices $\mathbb{B}^K$ and $\mathbb{L}^K$ and the *operator* $\mathcal{R}^K$ are the same than in the isotropic case. Finally, considering a nonzero source term and using the trace space operator $\mathcal{A}_{HDG}$, we obtain a global system similar to (4.13)

$$\sum_{K\in\mathcal{T}_h}(\mathcal{A}_{HDG}^K)^T\left[-\mathbb{B}^K(\mathbb{A}^K)^{-1}\mathbb{C}^K + \mathbb{L}^K\right]\mathcal{A}_{HDG}^K\underline{\Lambda} = \sum_{K\in\mathcal{T}_h} -(\mathcal{A}_{HDG}^K)^T\mathbb{B}^K(\mathbb{A}^K)^{-1}\mathbb{S}^K.$$

4.3 Boundary conditions

So far, we do not have described the discretization of the transmission condition on a boundary face. Before doing that, we remind the boundary conditions (2.4), (2.6) and (2.5) that we are considering

- Free surface condition over Γ_l : $\quad\underline{\underline{\sigma}}\cdot\mathbf{n} = 0$;
- Absorbing boundary condition over Γ_a : $\underline{\underline{\sigma}}\cdot\mathbf{n} + PA(\theta')P^T\mathbf{v} = 0$ where

- $P = \begin{pmatrix} n_x & -n_z \\ n_z & n_x \end{pmatrix}$;
- $A(\theta) = \begin{pmatrix} a_{11}(\theta) & a_{12}(\theta) \\ a_{21}(\theta) & a_{22}(\theta) \end{pmatrix}$ with

$$\begin{cases} a_{11}(\theta) &= -\rho v_p \dfrac{\kappa\cos^2\theta + \sin^2\theta}{\sqrt{\kappa^2\cos^2\theta + \sin^2\theta}} \left(\kappa\cos^2\theta + \sin^2\theta\right), \\ a_{12}(\theta) &= -\rho v_p \dfrac{\kappa\cos^2\theta + \sin^2\theta}{\sqrt{\kappa^2\cos^2\theta + \sin^2\theta}} \left(-(\kappa-1)\cos\theta\sin\theta\right), \\ a_{21}(\theta) &= -\rho v_p \dfrac{(\kappa-1)\cos\theta\sin\theta}{\sqrt{\kappa^2\cos^2\theta + \sin^2\theta}} \left(-(\kappa\cos^2\theta + \sin^2\theta)\right), \\ a_{22}(\theta) &= -\rho v_p \dfrac{(\kappa-1)\cos\theta\sin\theta}{\sqrt{\kappa^2\cos^2\theta + \sin^2\theta}} \left((\kappa-1)\cos\theta\sin\theta\right) - \rho v_s. \end{cases}$$

  To establish these expressions, we restrict ourselves to tilted transverse isotropic (TTI) media. The parameter θ is the tilted angle of the wave in the TTI medium, $\kappa = \sqrt{1-2\varepsilon}$, with ε one of Thomsen's constants defining the TTI nature of the medium and expressed by $\varepsilon = \dfrac{C_{11} - C_{13}}{2C_{33}}$.

- θ' is defined such as

$$\begin{cases} \cos\theta' = -n_z\sin\theta + n_x\cos\theta, \\ \\ \sin\theta' = \sqrt{1-\cos^2\theta'}. \end{cases}$$

In the isotropic case, $\theta = 0$ and thus the expression of matrix $A(\theta)$ is reduced to:

$$A(\theta) = \begin{pmatrix} -\rho v_p & 0 \\ 0 & -\rho v_s \end{pmatrix}.$$

The boundary conditions are taken into account in the last equation of the global formulation (3.11) and modify the expression of the transmission condition. Using the notation Bc for the matrix $PA(\theta')P^T$, we can write a general global formulation for both isotropic and anisotropic cases

$$\begin{aligned} \sum_{F\in\mathcal{F}_h\setminus\Gamma_l\cup\Gamma_a} \int_F \left(\widehat{\underline{\underline{\sigma}}}_h \cdot \mathbf{n}\right)\cdot\eta \;&+\; \sum_{F\in\Gamma_l}\int_F \left(\widehat{\underline{\underline{\sigma}}}_h\cdot\mathbf{n}\right)\cdot\eta \\ &+\; \sum_{F\in\Gamma_a}\int_F \left(\widehat{\underline{\underline{\sigma}}}_h\cdot\mathbf{n} + (Bc\lambda_h)\right)\cdot\eta \\ &=\; \sum_{F\in\Gamma_l}\int_F g_l\cdot\eta + \sum_{F\in\Gamma_a}\int_F g_a\cdot\eta, \end{aligned} \tag{4.17}$$

where in our case, $g_l = 0$ and $g_a = 0$. Replacing $\widehat{\underline{\underline{\sigma}}}_h\cdot\mathbf{n}$ by the expression (3.10), we obtain

$$\sum_{F\in\mathcal{F}_h}\int_F \left(\underline{\underline{\sigma}}_h\cdot\mathbf{n}\right)\cdot\eta - \sum_{F\in\mathcal{F}_h}\int_F \mathbf{S}\left(\mathbf{v}_h - \lambda_h\right)\cdot\eta + \sum_{F\in\Gamma_a}\int_F (Bc\lambda_h)\cdot\eta = 0. \tag{4.18}$$

Now, taking into account the boundary conditions in the transmission condition, the HDG formulation writes as, find $(\mathbf{v}_h, \underline{\underline{\sigma}}_h, \lambda_h) \in \mathbf{V}_h^p \times \mathbf{\Sigma}_h^p \times \mathbf{M}_h^0$ such that $\forall (\mathbf{w}, \underline{\underline{\xi}}, \eta) \in \mathbf{V}^p(K) \times \mathbf{\Sigma}^p(K) \times \mathbf{M}_h^0$

$$\left\{ \begin{array}{rcl} \displaystyle\sum_{K\in\mathcal{T}_h} \int_K i\omega\rho_K \mathbf{v}_h \cdot \mathbf{w} & - & \displaystyle\sum_{K\in\mathcal{T}_h} \int_K \left(\nabla \cdot \underline{\underline{\sigma}}_h\right) \cdot \mathbf{w} \\ & + & \displaystyle\sum_{K\in\mathcal{T}_h} \int_{\partial K} \mathbf{S}\left(\mathbf{v}_h - \lambda_h\right) \cdot \mathbf{w} = \sum_{K\in\mathcal{T}_h} \int_K \mathbf{f} \cdot \mathbf{w}, \\ \displaystyle\sum_{K\in\mathcal{T}_h} \int_K i\omega \underline{\underline{\sigma}}_h : \underline{\underline{\xi}} & + & \displaystyle\sum_{K\in\mathcal{T}_h} \int_K \mathbf{v}_h \cdot \nabla \cdot \left(\underline{\underline{C}}_K \underline{\underline{\xi}}\right) - \sum_{K\in\mathcal{T}_h} \int_{\partial K} \lambda_h \cdot \underline{\underline{C}}_K \underline{\underline{\xi}} \cdot \mathbf{n} = 0, \\ \displaystyle\sum_{F\in\mathcal{F}_h} \int_F \left(\underline{\underline{\sigma}}_h \cdot \mathbf{n}\right) \cdot \eta & - & \displaystyle\sum_{F\in\mathcal{F}_h} \int_F \mathbf{S}\left(\mathbf{v}_h - \lambda_h\right) \cdot \eta + \sum_{F\in\Gamma_a} \int_F (Bc\lambda_h) \cdot \eta = 0. \end{array} \right. \tag{4.19}$$

The discretization of the last equation of (4.19) on the boundary Γ_a is

$$\mathbb{Q}_{xl}^K \underline{\sigma}_{xx}^K + \mathbb{Q}_{zl}^K \underline{\sigma}_{xz}^K - \tau^{(K,l)} \mathbb{F}_l^K \underline{v}_x^K + \tau^{(K,l)} \mathbb{G}^j \underline{\lambda}_x^{\beta(K,l)} + Bc_{11} \mathbb{G}^F \underline{\lambda}_x^{\beta(k,l)} + Bc_{12} \mathbb{G}^F \underline{\lambda}_z^{\beta(k,l)} = 0, \tag{4.20}$$

and

$$\mathbb{Q}_{xl}^K \underline{\sigma}_{xz}^K + \mathbb{Q}_{zl}^K \underline{\sigma}_{zz}^K - \tau^{(K,l)} \mathbb{F}_l^K \underline{v}_z^K + \tau^{(K,l)} \mathbb{G}^j \underline{\lambda}_z^{\beta(K,l)} + Bc_{22} \mathbb{G}^F \underline{\lambda}_z^{\beta(k,l)} + Bc_{21} \mathbb{G}^F \underline{\lambda}_x^{\beta(k,l)} = 0. \tag{4.21}$$

The expressions of Bc's coefficients in the isotropic case are given by

$$Bc_{11} = -\rho \left(v_p^K n_x^{K^2} + v_s^K n_z^{K^2}\right),$$

$$Bc_{12} = Bc21 = -\rho n_x^K n_z^K \left(v_p^K - v_s^K\right),$$

$$Bc_{22} = -\rho \left(v_p^K n_z^{K^2} + v_s^K n_x^{K^2}\right).$$

For an element having a face on the absorbing boundary, the matrix $\mathbb{B}^K$ is not modified, whereas matrix $\mathbb{L}^K$ becomes, for example if the edge $l = 1$ of K is an absorbing edge,

$$\mathbb{L}^K = \begin{bmatrix} \left(\tau^{(K,1)} + Bc_{11}\right) \mathbb{G}^{\beta(K,1)} & 0 & 0 & Bc_{12}\mathbb{G}^{\beta(K,1)} & 0 & 0 \\ 0 & \tau^{(K,2)}\mathbb{G}^{\beta(K,)} & 0 & 0 & 0 & 0 \\ 0 & 0 & \tau^{(K,3)}\mathbb{G}^{\beta(K,3)} & 0 & 0 & 0 \\ Bc_{21}\mathbb{G}^{\beta(K,1)} & 0 & 0 & \left(\tau^{(K,1)} + Bc_{22}\right) \mathbb{G}^{\beta(K,1)} & 0 & 0 \\ 0 & 0 & 0 & 0 & \tau^{(K,2)}\mathbb{G}^{\beta(K,2)} & 0 \\ 0 & 0 & 0 & 0 & 0 & \tau^{(K,3)}\mathbb{G}^{\beta(K,3)} \end{bmatrix}.$$

5 2D numerical results

In this section, we provide some numerical results in 2D to assess the performances (accuracy and efficiency) of the proposed HDG scheme. This scheme has been implemented in a Fortran 90 software.

We use the MUMPS sparse direct solver for the resolution of the linear system (see [10] for more details) resulting from the HDG discretization scheme.

Numerical experiments are performed on a hardware system equipped with 2 quad-core Nehalem Intel® Xeon® X5550/2,66 GHz CPUs and 24Go (DDR3 1333 MHz) of RAM.

Two simple problems, the propagation of a plane wave in a homogeneous medium and the scattering of a plane wave by a disk, and one heterogeneous problem, the scattering of a plane wave by a solid disk, are considered. We remind that to propagate the waves we have to solve the elastic Helmholtz equations. For each test problem, we compare the HDG results with those obtained with a nodal DG method, the upwind flux DG method [].

5.1 Plane wave propagation in an homogeneous medium

We first consider the simple test problem of the propagation of a plane wave in an homogeneous medium. The computational domain Ω is a 10000 m $\times$10000 m square. The physical properties of the medium are $\rho = 1000$ kg.m^{-3} and values of Lamé's coefficients λ and μ that are set to 8 MPa and 4 MPa respectively. These values imply a velocity v_p of P-waves equal to 4000 m.s^{-1} and a velocity v_s of S-waves equal to 2000 m.s^{-1}. On the boundaries we impose an absorbing condition with a plane wave incident field

$$U = \nabla e^{i(k_x \cos\theta x + k_z \sin\theta z)} = \begin{pmatrix} V_{x0} \\ V_{z0} \\ \sigma_{xx0} \\ \sigma_{zz0} \\ \sigma_{xz0} \end{pmatrix} e^{i(k_x \cos\theta x + k_z \sin\theta z)},$$

where $k = \sqrt{k_x^2 + k_z^2} = \dfrac{\omega}{v_p}$ is the wavenumber, $k_x = \dfrac{\omega}{v_p}\cos\theta$ and $k_z = \dfrac{\omega}{v_p}\sin\theta$, and θ is the incidence angle. Here, ω denotes the angular frequency, $\omega = 2\pi f$ where f is the frequency. If we choose arbitrarily V_{x0}, we can express the other components as

$$\begin{cases} V_{z0} = \dfrac{k_x k_z \left(\lambda + \mu\right)}{\rho\omega^2 - k_x^2\mu - k_z^2\lambda + 2\mu)} V_{x0} \\ \sigma_{xx0} = \dfrac{-1}{\omega}\left(k_x \left(\lambda + 2\mu\right) V_{x0} + \lambda k_z V_{z0}\right) \\ \sigma_{zz0} = \dfrac{-1}{\omega}\left(\lambda k_x V_{x0} + \left(\lambda + 2\mu\right) k_z V_{z0}\right) \\ \sigma_{xz0} = \dfrac{-\mu}{\omega}\left(k_z V_{x0} + k_x V_{z0}\right). \end{cases}$$

In the simulations we choose θ=0 and $f = 2$ Hz, so that $\omega = 4\pi \simeq 12.56$ rad.s^{-1}. We discretize the computational domain Ω into three unstructured meshes with respectively 3000, 10 000 and 45 000 elements. Two of these meshes are shown on figs. 5.1 and 5.2; their characteristics are given in tab. 5.1. The last mesh is too fine to be represented.

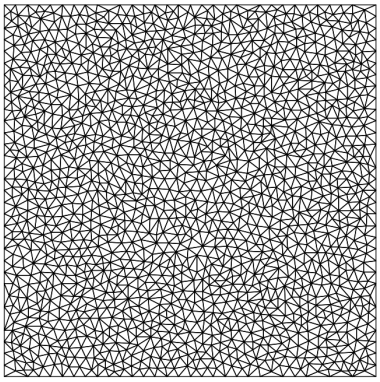

Figure 5.1: Discretization of Ω: mesh M1, 3000 elements.

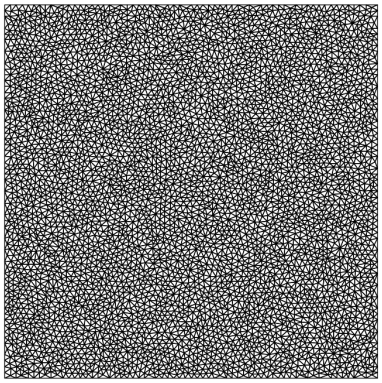

Figure 5.2: Discretization of Ω: mesh M2, 10000 elements.

Mesh	# Mesh elements	# Mesh vertices	h_{min}	h_{max}	h_{min}/h_{max}
M1	3100	1620	193.6	625.0	3.2
M2	10 300	5200	107.5	312.5	2.9
M3	45 000	22 500	45.4	156.2	3.5

Table 5.1: Characteristics of the three meshes.

We compare the obtained numerical solutions by focusing on the V_x component. When using the coarsest mesh with 3000 triangles and the HDG-$\mathbb{P}_1$ formulation, we obtain the numerical solution shown on fig. 5.4. On fig. 5.5, we compare this numerical solution to the exact one represented on fig. 5.3. Clearly, for this relatively coarse mesh, the HDG-$\mathbb{P}_1$ scheme is not enough accurate. Increasing the interpolation degree (fig. 5.6) leads to a numerical solution which is closer to the exact one. If we increase the resolution of the mesh (fig. 5.8), the numerical solution is closer too to the exact one but we clearly see that the second mesh is not again well adapted for the HDG-$\mathbb{P}_1$ scheme with our choices of parameters for this test problem.

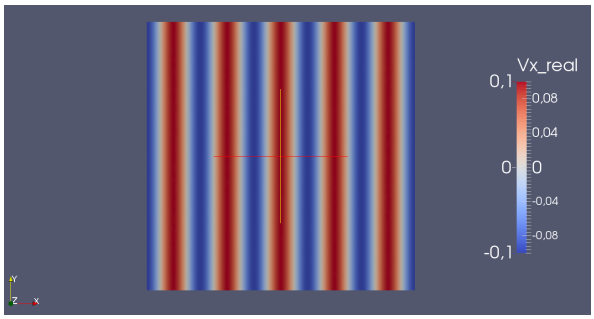

Figure 5.3: Exact solution, V_x component.

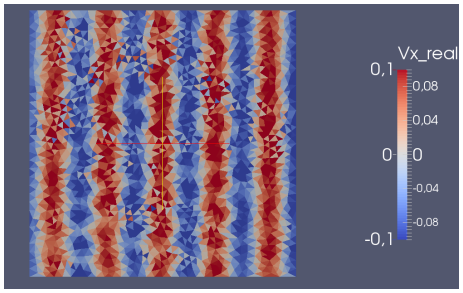

Figure 5.4: Numerical solution, mesh M1, HDG-$\mathbb{P}_1$ scheme, V_x component.

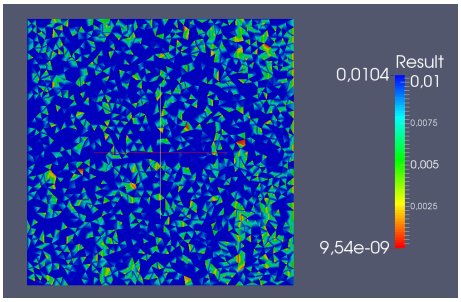

Figure 5.5: Absolute error between the exact solution and the solution computed with the HDG-$\mathbb{P}_1$ scheme on mesh M1.

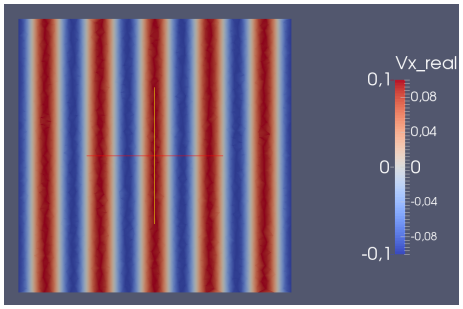

Figure 5.6: Numerical solution, mesh M1, HDG-$\mathbb{P}_2$ scheme, V_x component.

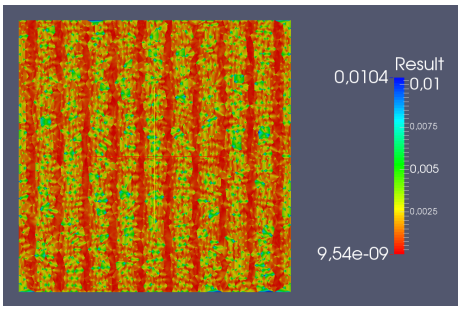

Figure 5.7: Absolute error between the exact solution and the solution computed with the HDG-$\mathbb{P}_2$ scheme on mesh M1.

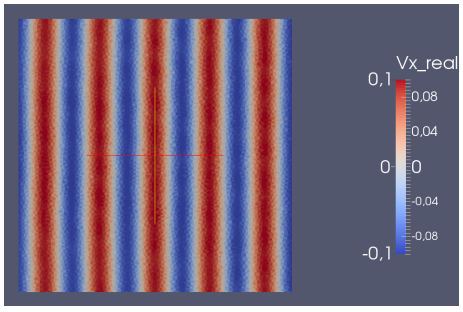

Figure 5.8: Numerical solution, mesh M2, HDG-$\mathbb{P}_1$ scheme, V_x component.

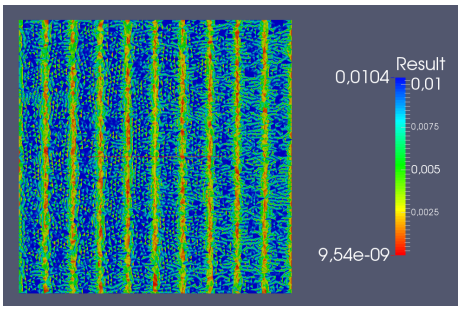

Figure 5.9: Absolute error between the exact solution and the solution computed with the HDG-$\mathbb{P}_1$ scheme on mesh M2.

Fig. 5.10 shows the numerical convergence of the HDG method. As with classical finite element methods or with the upwind flux based DGFD method, we observe a convergence with order $p+1$ when the interpolation order is p, i.e with optimal rate.

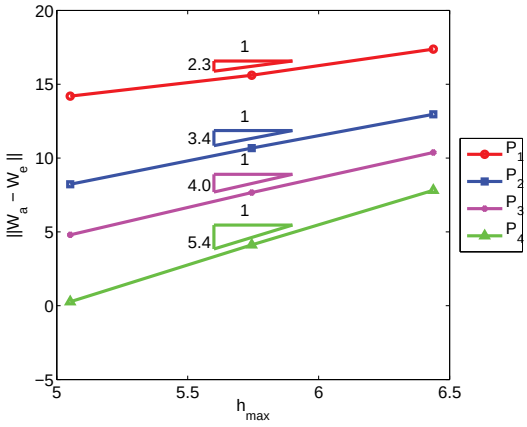

Figure 5.10: Convergence order of HDG method for plane wave propagation in a homogeneous medium.

Tabs. 5.2 and 5.3 compare the mean and the relative errors obtained using the HDG formulation and the upwind flux based DG formulation for the V_x and σ_{xx} components respectively. If we focus on the V_x component, the error, mean or relative, is larger with the HDG scheme for given mesh resolution and interpolation order. However, if we compare both methods for a target accuracy, see tab. 5.4, using the same mesh, the HDG method requires one interpolation order more than the upwind flux based DG method (UDG in tabs. 5.4 and 5.5) but is less expensive in terms of memory consumption. In tab. 5.5 we use the same interpolation order for the two schemes: the HDG method needs a more refined mesh than the UDG method, but, except when the the interpolation degree is equal to 1, it is still less expensive from the point of view of memory space. For a same accuracy the computational time is quite the same for both methods.

When we compare both methods on the same mesh and with the same interpolation order, in terms of memory requirement (see tab. 5.6) and computational time (see tab. 5.7), the HDG method is more efficient as a result of the fact that the HDG method leads to a discrete system with a lower number of globally coupled unknowns in comparsion to the classical DG method. If we consider an uniform interpolation degree (i.e. same interpolation degree for all the elements), for the 2D elastic Helmholtz equations, in the classical DG framework we have, $N_{DG} = 5 \times nde \times N_e$ globally coupled unknowns, where nde is the number of degrees of freedom in each element and N_e is the number of elements, whereas this number of unknowns with the HDG method is $N_{HDG} = 5 \times ndf \times N_f$, where ndf is the number of degrees of freedom on each face (edge in 2D) and N_f is the number of faces. Moreover, $ndf = p + 1$, $nde = \dfrac{(p+1)(p+2)}{2}$, and $N_f \approx \dfrac{3}{2} N_e$. The number of unknowns which corresponds to the number of degrees of freedom (dof) for each method is given in tab. 5.8. We also give the number of dof per wavelength (λ_w) which is for the considered test problem equal to 2000 m (we recall that $\lambda_w = \dfrac{v_p}{f}$). We observe that for a given error level, for instance 10^{-3} on the V_x component, using the mesh M1 (3100 elements), the upwind DG-$\mathbb{P}_1$ scheme requires 9.4 10^4 unknowns while the HDG-$\mathbb{P}_2$ scheme leads to a number of unknowns equal to 3.8 10^4, i.e. 3 times less unknowns.

For this test problem, we also look at the pattern of the global matrix of each method, fig. 5.11 for the HDG method and fig. 5.12 for the upwind flux DG method. We clearly see that the two matrices are sparse matrices as expected. For example, for the mesh M2, the fill rate of the HDG-$\mathbb{P}_2$ matrix is 0.038% and the one of the DG-$\mathbb{P}_2$ matrix is 0.015%. The advantage of the upwind DG matrix is that it is more sparse than the HDG one, but its size is larger (approximately 3 times bigger).

The condition numbers of these global matrices are represented on fig. 5.13 to 5.16 for each interpolation degree and for different frequencies (from 1 Hz to 8 Hz).

h (m)	Interpolation degree	Mean Error V_x		Relative Error V_x	
		HDG scheme	Upw. scheme	HDG scheme	Upw. scheme
625.0	1	1.6	1.8e-02	52.8	6.0
312.5	1	0.1	1.7e-03	13.7	1.8
56.25	1	1.2e-2	9.9e-05	5.5	0.4
625.0	2	6.7e-2	1.6e-03	2.1	0.5
312.5	2	5.9e-3	5.7e-05	0.6	5.8e-02
56.25	2	3.1e-4	1.4e-06	0.1	6.1e-03
625.0	3	5.4e-3	1.3e-04	0.2	4.1e-02
312.5	3	2.6e-4	3.1e-06	2.7e-2	3.2e-03
56.25	3	6.5e-6	3.7e-08	2.9e-3	1.7e-04
625.0	4	3.9e-4	1.0e-05	1.2	3.2e-03
312.5	4	9.5e-6	6.8e-08	9.7e-4	7.0e-05
56.25	4	1.1e-7	3.1e-10	4.9e-5	1.4e-06

Table 5.2: Mean and relative errors on V_x.

h (m)	Interpolation degree	Mean Error σ_{xx}		Relative Error σ_{xx}		Convergence order	
		HDG scheme	Upw. scheme	HDG scheme	Upw. scheme	HDG scheme	Upw. scheme
625.0	1	4721.2	72.9	38.8	6.0	-	-
312.5	1	333.8	6.6	8.7	1.7	2.5	1.7
56.25	1	19.6	0.4	2.2	0.4	2.0	2.0
625.0	2	64.4	5.9	0.5	0.5	-	-
312.5	2	1.9	0.3	5.0e-2	6.5e-02	3.3	2.9
56.25	2	3.6e-2	6.2e-03	4.0e-3	6.9e-03	3.5	3.2
625.0	3	4.1	0.4	3.2e-2	3.1e-02	-	-
312.5	3	8.7e-2	1.0e-02	2.2e-3	2.7e-03	3.9	3.7
56.25	3	1.2e-3	1.4e-04	1.4e-4	1.5e-04	4.1	4.2
625.0	4	0.3	3.4e-02	2.7e-3	2.7e-03	-	-
312.5	4	2.8e-3	3.1e-04	7.1e-5	7.9e-05	5.3	5.2
56.25	4	1.4e-5	1.5e-06	1.5e-6	1.7e-06	5.6	5.6

Table 5.3: Mean and relative errors on σ_{xx} and convergence order.

Error	# Mesh elements	Interpolation degree		Memory (MB)		Construction time (s)		Solution time (s)	
		HDGm	UDGm	HDGm	UDGm	HDGm	UDGm	HDGm	UDGm
1e-02	3100	2	1	97	288	1.3	4.0e-02	0.6	1.5
1e-03	3100	3	2	170	804	4.8	0.1	1.0	6.0
1e-03	10300	2	1	355	1076	2.8	0.1	2.3	7.2
1e-04	3100	4	3	254	1656	5.8	0.2	1.6	14.4

Table 5.4: Comparison between computational time and memory requirement for the same mesh.

Error	Interpolation degree	# Mesh elements		Memory (MB)		Construction time (s)		Solution time (s)	
		HDGm	UDGm	HDGm	UDGm	HDGm	UDGm	HDGm	UDGm
1e-02	1	45000	3100	797	288	3.3	4.0e-02	6.1	1.5
1e-03	2	10300	3100	355	804	2.8	0.1	2.3	6.0
1e-04	3	10300	3100	624	1656	8.1	0.2	4.4	14.4

Table 5.5: Comparison between computational time and memory requirement for the same interpolation order.

# Mesh elements	Interpolation degree	Non-zeros terms		Memory (MB)	
		HDG scheme	Upw. scheme	HDG scheme	Upw. scheme
3100	1	4.5e+05	1.5e+06	44	288
10300	1	1.5e+06	5.1e+06	161	1076
45000	1	6.4e+06	2.2e+07	797	5492
3100	2	1.0e+06	4.3e+06	97	804
10300	2	3.3e+06	1.4e+07	355	3097
45000	2	1.4e+07	6.2e+07	1746	15965
3100	3	1.8e+06	9.4e+06	170	1656
10300	3	5.9e+06	3.1e+07	624	6600
45000	3	2.6e+07	1.3e+08	3080	34597
3100	4	2.8e+06	1.8e+07	254	2749
10300	4	9.2e+06	5.9e+07	947	10098
45000	4	4.0e+07	2.6e+08	4653	50297

Table 5.6: Number of non-zero terms in the global matrix and memory used.

# Mesh elements	Interpolation degree	Construction time (s)		Solution time (s)	
		HDG scheme	Upw. scheme	HDG scheme	Upw. scheme
3100	1	0.2	4.0e-02	0.2	1.5
10300	1	0.8	0.1	1.0	7.2
45000	1	3.3	0.7	6.1	68.0
3100	2	1.3	0.1	0.6	6.0
10300	2	2.8	0.3	2.3	28.8
45000	2	12.2	1.5	15.4	224.5
3100	3	4.8	0.2	1.0	14.4
10300	3	8.1	0.8	4.4	78.2
45000	3	35.8	3.4	32.2	643.2
3100	4	5.8	0.5	1.6	28.1
10300	4	21.1	1.8	8.7	135.2
45000	4	106.1	7.6	70.7	1077.4

Table 5.7: Time required for the global matrix construction and for the system resolution.

# Mesh elements	Interpolation degree	# dof		#dof/wavelength	
		HDG scheme	Upw. scheme	HDG scheme	Upw. scheme
3100	1	1.9e+04	4.7e+04	9	23
10300	1	6.2e+04	1.5e+05	31	77
45000	1	2.7e+05	6.7e+05	134	334
3100	2	2.8e+04	9.4e+04	14	46
10300	2	9.3e+04	3.1e+05	46	154
45000	2	4.0e+05	1.3e+06	201	668
3100	3	3.8e+04	1.6e+05	19	78
10300	3	1.2e+05	5.1e+05	62	256
45000	3	5.4e+05	2.2e+06	268	1114
3100	4	4.7e+04	2.3e+05	23	117
10300	4	1.5e+05	7.7e+05	77	384
45000	4	6.7e+05	3.3e+06	335	1671

Table 5.8: Total number of dof and number of dof per wavelength (λ_w).

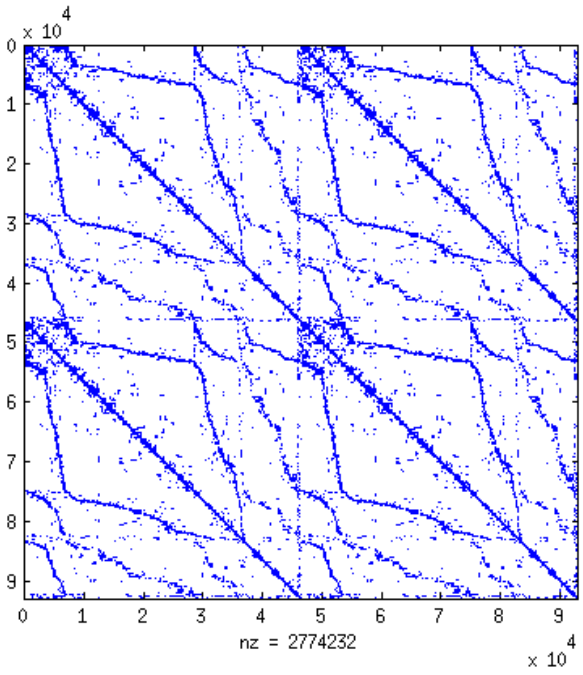

Figure 5.11: Pattern of the HDG matrix for mesh M2 and an interpolation degree $p = 2$.

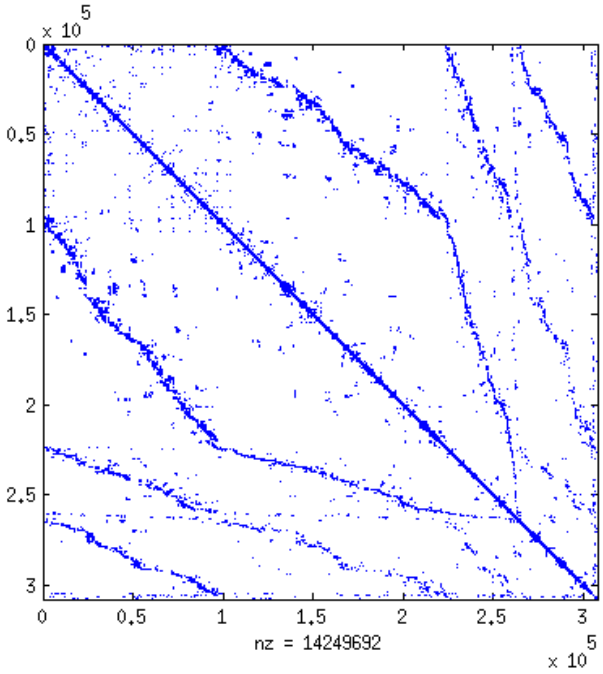

Figure 5.12: Pattern of the upwind flux DG matrix for mesh M2 and an interpolation degree $p = 2$.

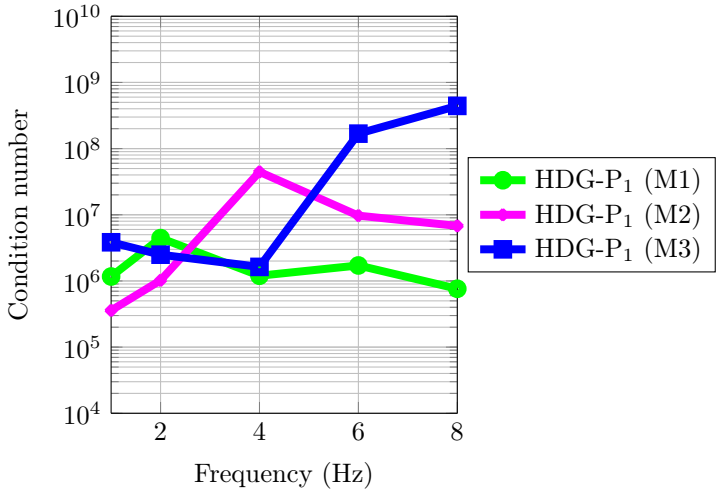

Figure 5.13: Condition number of the HDG-$\mathbb{P}_1$ matrix as a function of the frequency.

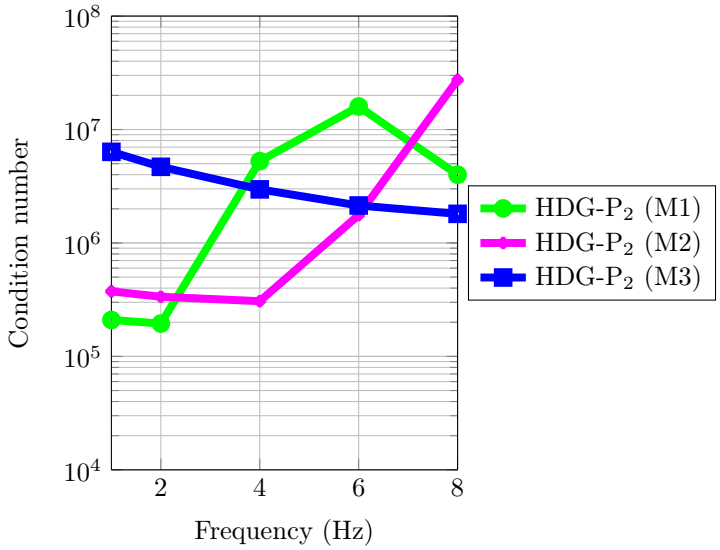

Figure 5.14: Condition number of the HDG-$\mathbb{P}_2$ matrix as a function of the frequency.

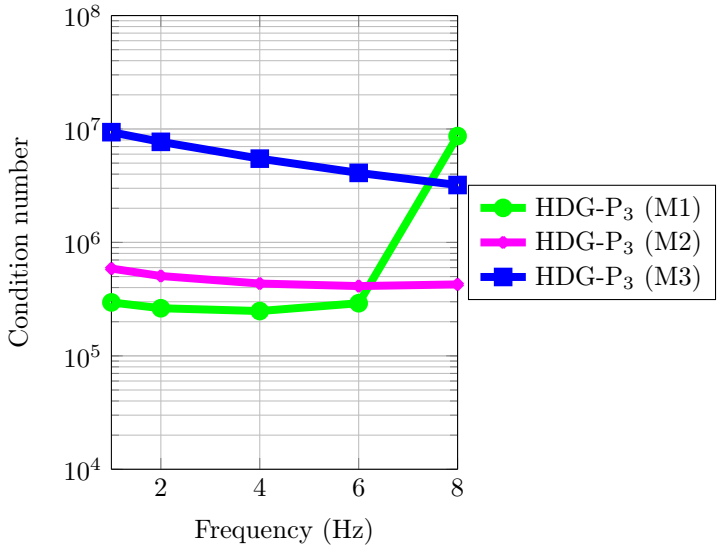

Figure 5.15: Condition number of the HDG-$\mathbb{P}_3$ matrix as a function of the frequency.

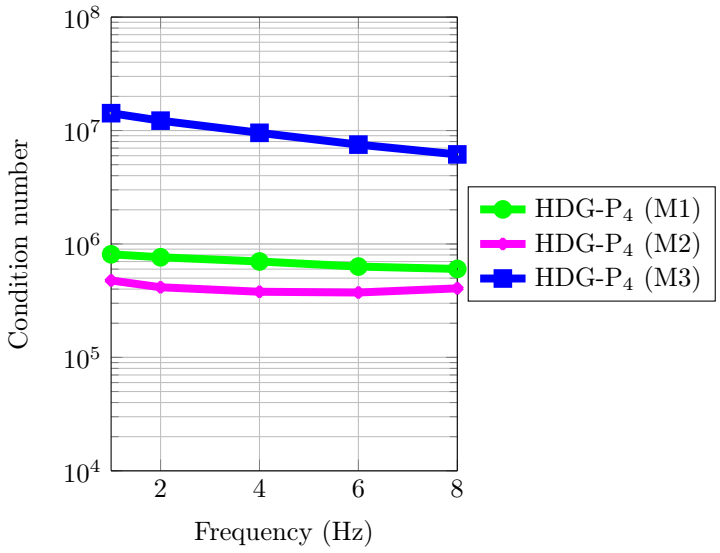

Figure 5.16: Condition number of the HDG-$\mathbb{P}_4$ matrix as a function of the frequency.

5.2 Disk-shaped scatterer

We consider now the problem of the scattering of a plane wave by an infinite elastic cylinder. The computational domain Ω is the ring included between the circle of radius $a = 2000$ m whose boundary is Γ_a and the concentric circle of radius $b = 8000$ m whose the boundary Γ_b is assume to be an artificial boundary (see fig. 5.17). On the boundary Γ_a we apply the free condition (2.4); on Γ_b we apply the absorbing condition (2.6) in order to simulate an infinite isotropic medium. The homogeneous material is characterized by a mass density $\rho = 1.10^3$ kg.m^{-3} and Lamé's coefficients $\lambda = 8$ MPa and $\mu = 4$ MPa, which imply a P-waves velocity v_p equal to 4.010^3 m.s^{-1} and a $S-$waves velocity v_s equal to 2.010^3 m.s^{-1}. The distance between the two circles of radius a and b is such that it corresponds to 1.5 times the wavelength λ_o. We remind that $\lambda_o = \frac{v_p}{f}$, where f is the frequency. Here, f is chosen equal to 4Hz.

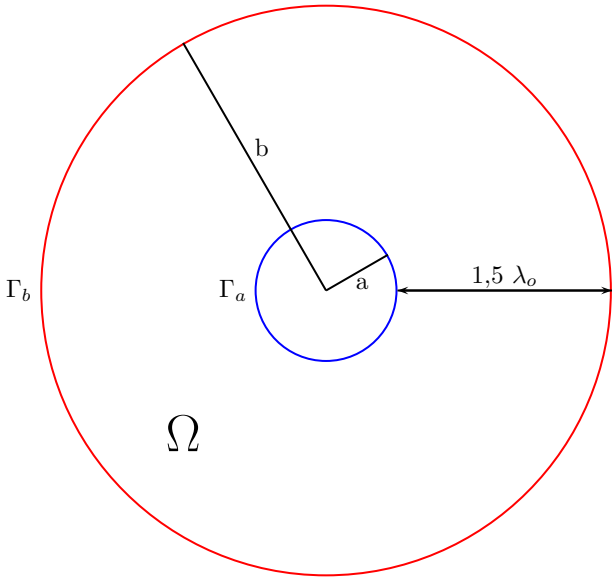

Figure 5.17: Configuration of the computational domain Ω for the elastic disk-shaped scatterer.

We discretize the computational domain Ω thanks to three unstructured meshes with respectively 1200, 5100 and 21 000 elements. Two of these meshes are shown on figs. 18(a) and 18(b); their characteristics are given in tab. 5.9.

Mesh	# Mesh elements	# Mesh vertices	h_{min}	h_{max}	h_{min}/h_{max}
M1	1200	640	440.5	1016.9	2.3
M2	5100	2630	212.4	490.1	2.3
M3	21 000	11 000	105.9	245.9	2.3

Table 5.9: Characteristics of the three meshes

We plot the exact solution of the scattering problem for the V_x component on fig. 5.19. The corresponding numerical solution computed on the second mesh and using the HDG-$\mathbb{P}_2$ method is shown

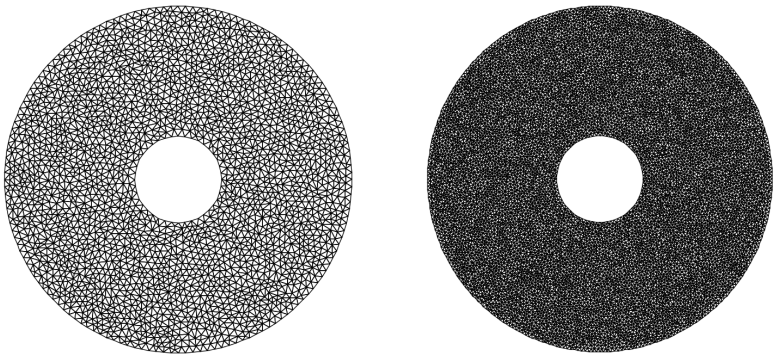

(a) Mesh M1, 1200 elements. (b) Mesh M2, 5100 elements.

Figure 5.18: Discretization of the computational domain Ω for the elastic disk-shaped scatterer.

on fig. 20(a). This numerical solution is not enough accurate and suitable, its comparison with the exact solution is given on fig. 20(b). To obtain a better numerical solution, we can increase the interpolation order, using the same mesh (see fig. 20(c)) or we can use a finer mesh (see fig. 20(e)).

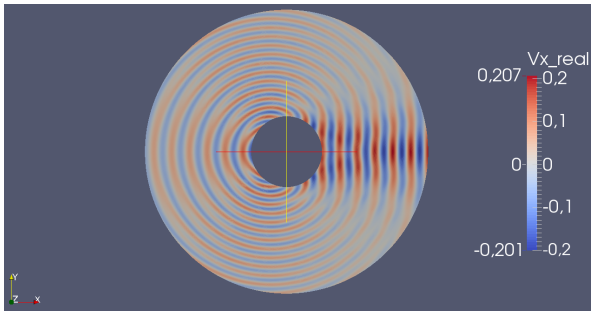

Figure 5.19: Exact solution, V_x component.

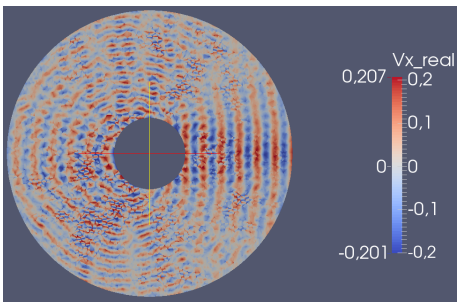

(a) Numerical solution, mesh M2, HDG-$\mathbb{P}_2$ scheme, V_x component.

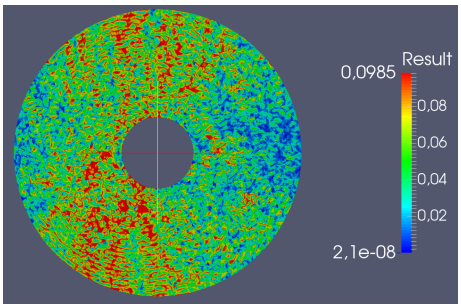

(b) Absolute error between the exact solution and the solution computed with HDG-$\mathbb{P}_2$ scheme, mesh M2.

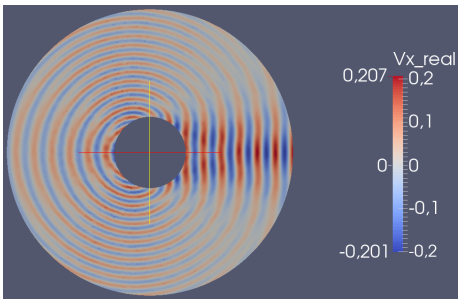

(c) Numerical solution, mesh M2, HDG-$\mathbb{P}_3$ scheme, V_x component.

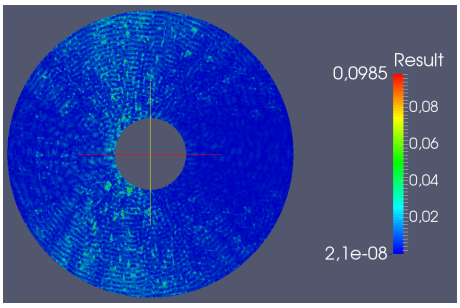

(d) Absolute error between the exact solution and the solution computed with HDG-$\mathbb{P}_3$ scheme, mesh M2.

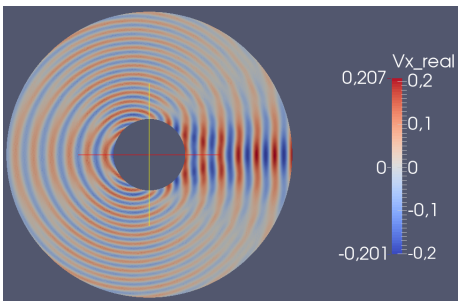

(e) Numerical solution, mesh M3, HDG-$\mathbb{P}_2$ scheme, V_x component.

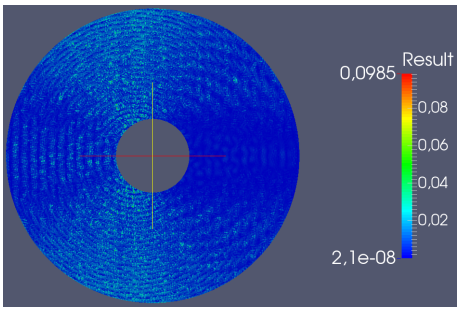

(f) Absolute error between the exact solution and the solution computed with HDG-$\mathbb{P}_2$ scheme, mesh M3.

The numerical convergence is presented on fig. 5.20. We also plot the numerical convergence of the upwind DG method on fig. 5.21. We remark that we do not obtain the expected convergence orders for both schemes, and that the two schemes behave similarly. This is probably due to the fact that the geometric error dominates. Indeed, for this test problem, the curved boundaries are discretized by affine elements which a limitation for obtaining higher convergence orders.

When we compare the mean and relative errors for V_x and σ_{xx} components (see tables 5.10 and 5.11), we observe that, except for the coarsest mesh (mesh M1), we obtain the same error level for both methods. When we compare the memory requirement (see table 5.12) and the computational time (see table 5.14) we note that the HDG scheme requires less memory than the upwind DG method (around 10 times less for this test problem). The construction of the HDG global matrix requires more time than the one of the upwind DG method but this additional time is drastically compensated by the resolution time. Finally, as with the previous test problem, the HDG method requires less computational time for a whole simulation than the upwind DG method.

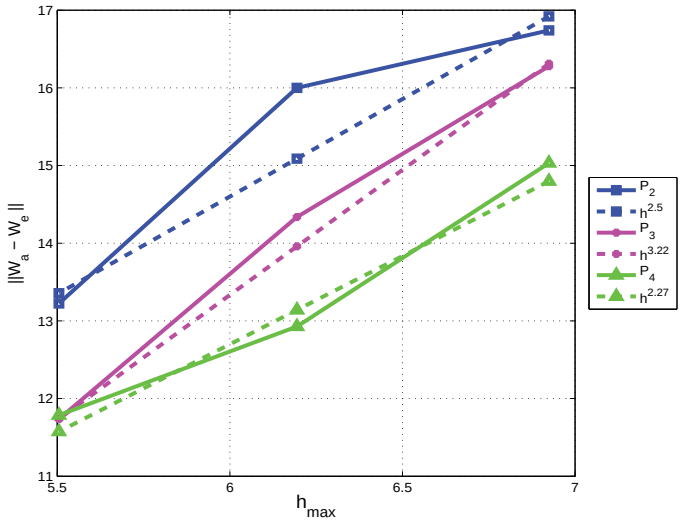

Figure 5.20: Numerical convergence of the HDG method.

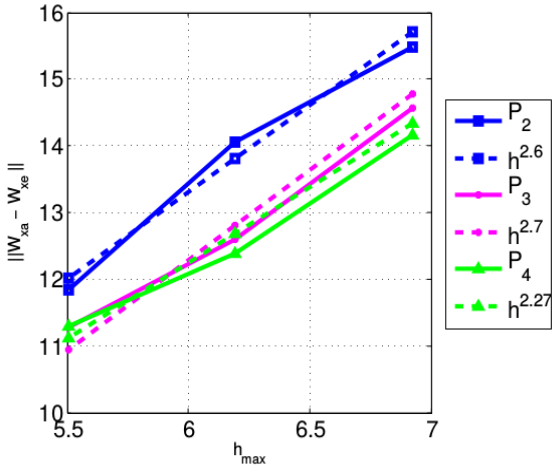

Figure 5.21: Numerical convergence of the upwind flux DG method.

h (m)	Interpolation degree	Mean Error V_x		Relative Error V_x	
		HDG scheme	Upw. scheme	HDG scheme	Upw. scheme
1016.9	2	2.2	1.0	273.4	123.4
490.1	2	0.3	8.1e-02	122.7	36.8
245.9	2	6.3e-03	1.8e-03	11.1	3.2
1016.9	3	1.5	0.5	154.2	56.4
490.1	3	2.5e-02	1.6e-02	10.9	7.2
245.9	3	1.0e-03	9.6e-04	1.8	1.7
1016.9	4	0.5	0.4	48.5	37.3
490.1	4	1.2e-02	1.3e-02	5.4	5.5
245.9	4	9.9e-04	9.9e-04	1.7	1.7

Table 5.10: Mean and relative errors on V_x.

h (m)	Interpolation degree	Mean Error σ_{xx}		Relative Error σ_{xx}		Convergence order	
		HDG scheme	Upw. scheme	HDG scheme	Upw. scheme	HDG scheme	Upw. scheme
625.0	2	7101.5	3802.5	242.7	128.0	-	-
312.5	2	635.5	159.8	83.3	20.9	1.0	2.0
56.25	2	9.9	4.8	5.1	2.5	4.0	3.2
625.0	3	3687.6	1195.1	111.8	36.3	-	-
312.5	3	43.7	37.9	5.6	4.9	4.0	2.7
56.25	3	2.9	3.0	1.5	1.5	2.3	1.9
625.0	4	1033.4	743.8	31.0	22.3	-	-
312.5	4	30.2	31.0	3.9	3.4	2.9	2.4
56.25	4	2.9	3.0	1.5	1.5	1.6	1.6

Table 5.11: Mean and relative errors on σ_{xx} and convergence order.

# Mesh elements	Interpolation degree	Non-zeros terms		Memory (MB)	
		HDG scheme	Upw. scheme	HDG scheme	Upw. scheme
1200	2	3.9e+05	1.6e+06	44	269
5100	2	1.6e+06	7.0e+06	179	1360
21000	2	6.6e+06	2.7e+07	783	6578
1200	3	6.9e+05	3.6e+06	70	525
5100	3	2.9e+06	1.5e+07	309	2921
21000	3	1.2e+07	6.2e+07	1384	14131
1200	4	1.1e+06	6.8e+06	100	895
5100	4	4.6e+06	2.9e+07	462	4537
21000	4	1.8e+07	1.2e+08	2101	21186

Table 5.12: Number of non-zero terms in the global matrix and memory used.

# Mesh elements	Interpolation degree	# dof		#dof/wavelength	
		HDG scheme	Upw. scheme	HDG scheme	Upw. scheme
1200	2	1.1e+04	3.6e+04	11	35
5100	2	4.6e+04	1.5e+05	46	152
21000	2	1.8e+05	6.1e+05	184	611
1200	3	1.5e+04	6.0e+04	14	59
5100	3	6.1e+04	2.5e+05	61	253
21000	3	2.5e+05	1.0e+06	246	1018
1200	4	1.8e+04	8.9e+04	18	89
5100	4	7.7e+04	3.8e+05	77	380
21000	4	3.1e+05	1.5e+06	307	1527

Table 5.13: Total number degrees of freedom (ndof) and ndof per wavelength (λ_w).

# Mesh elements	Interpolation degree	Construction time(s)		Solution time (s)	
		HDG scheme	Upw. scheme	HDG scheme	Upw. scheme
1200	2	0.4	7.1e-2	0.3	2.6
5100	2	1.5	0.3	1.7	14.7
21000	2	5.5	1.2	12.0	93.7
1200	3	1.1	0.2	0.6	5.3
5100	3	4.3	0.7	3.4	38.2
21000	3	16.5	2.7	26.4	249.3
1200	4	2.8	0.3	0.9	10.2
5100	4	10.9	1.4	6.2	65.6
21000	4	43.7	5.5	49.5	447.3

Table 5.14: Time required for the global matrix construction and for the system resolution.

5.3 Elastic scattering

Finally we consider the problem of the scattering of a plane wave by an elastic solid in an infinite circle, which corresponds to an heterogeneous wave propagation problem. The computational domain $\Omega = \Omega_a \cup \Omega_b$ is represented on fig. 5.22. It is composed of the circle Ω_a and the ring Ω_b. We have two materials: the first material in Ω_b has a mass density $\rho = 1.0$ kg.m^{-3} and Lamé's coefficients $\lambda = 8.0$ MPa and $\mu = 4.0$ MPa; the second material in Ω_a has a mass density $\rho = 2.0$ kg.m^{-3} and Lamé's coefficients $\lambda = 6.4\ 10^1$ MPa and $\mu = 3.2\ 10^1$ MPa. These values imply a $P-$waves velocity v_p equal to $4.0\ 10^3$ m.s^{-1} in Ω_b and to $8.0\ 10^3$ m.s^{-1} in Ω_a, and a $S-$waves velocity v_s equal to $2.0\ 10^3$ m.s^{-1} in Ω_b and to $4.0\ 10^3$ m.s^{-1} in Ω_a.

We discretize the computational domain Ω into three unstructured meshes with respectively 1300, 5400 and 22 000 elements. Two of these meshes are shown on figs. 23(a) and 23(b); their characteristics are given in table 5.15.

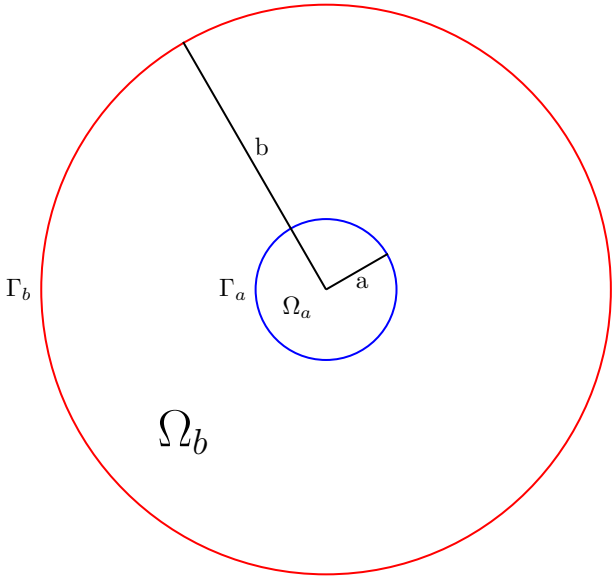

Figure 5.22: Configuration of the computational domain Ω for the elastic solid scatterer.

Mesh	# Mesh elements	# Mesh vertices	h_{min}	h_{max}	h_{min}/h_{max}
M1	1300	700	440.5	1016.9	2.3
M2	5400	2800	211.6	490.1	2.3
M3	22 000	11 000	105.9	245.9	2.3

Table 5.15: Characteristics of the three meshes

Similarly to the two previous homogeneous test problems, we plot the exact solution of V_x component (see fig. 5.24). On fig. 25(a) we plot the numerical solution for V_x component computed with the HDG-$\mathbb{P}_2$ scheme on mesh M2; then we increase the interpolation order using the same mesh, fig. 26(a), or refine the mesh while maintening unchanged the interpolation order, fig. 27(a).

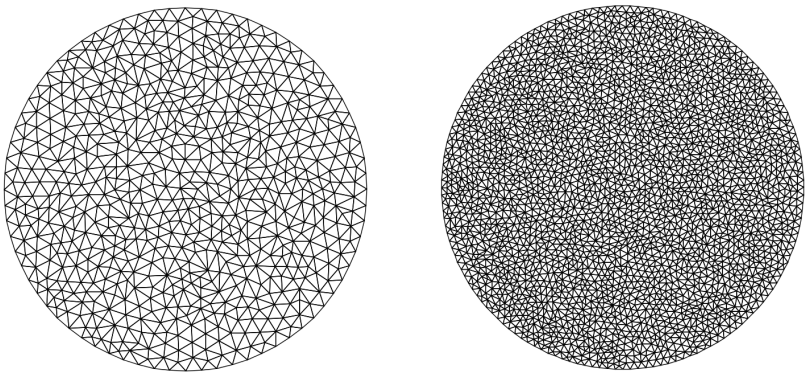

(a) Mesh M1, 1300 elements. (b) Mesh M2, 5400 elements.

Figure 5.23: Discretization of the computational domain Ω for the elastic solid scatterer.

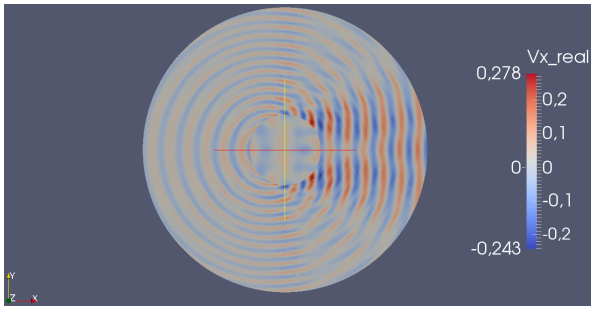

Figure 5.24: Exact solution, V_x component.

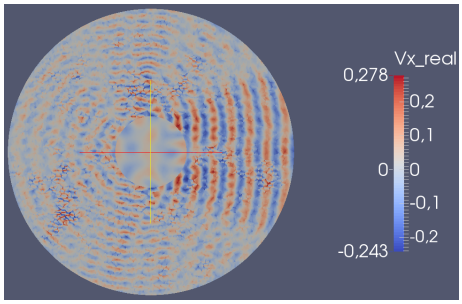

(a) Numerical solution, mesh M2, HDG-$\mathbb{P}_2$ scheme, V_x component.

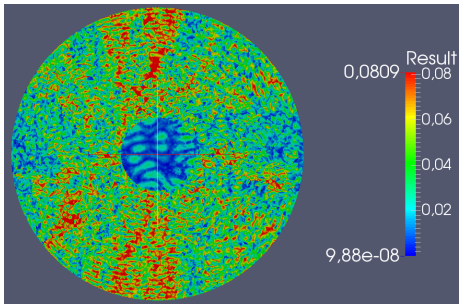

(b) Absolute error between the exact solution and the solution computed with HDG-$\mathbb{P}_2$ scheme, mesh M2.

Figure 5.25: HDG-$\mathbb{P}_2$ scheme, mesh M2

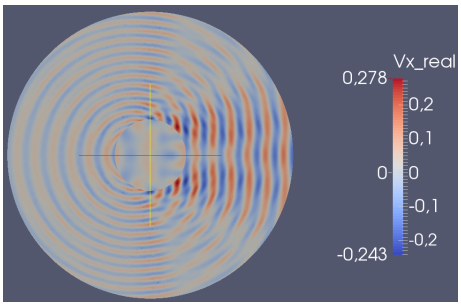

(a) Numerical solution, mesh M2, HDG-$\mathbb{P}_3$ scheme, V_x component.

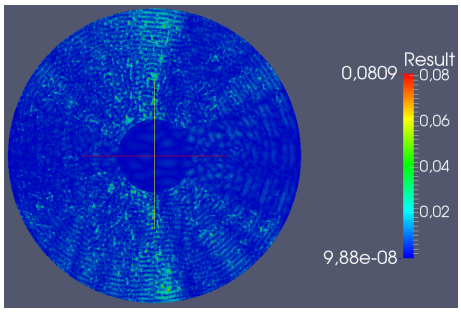

(b) Absolute error between the exact solution and the solution computed with HDG-$\mathbb{P}_3$ scheme, mesh M2.

Figure 5.26: Numerical solution, mesh M2, HDG-$\mathbb{P}_3$ scheme, V_x component.

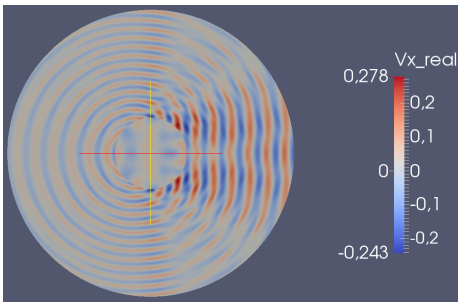

(a) Numerical solution, mesh M3, HDG-$\mathbb{P}_2$ scheme, V_x component.

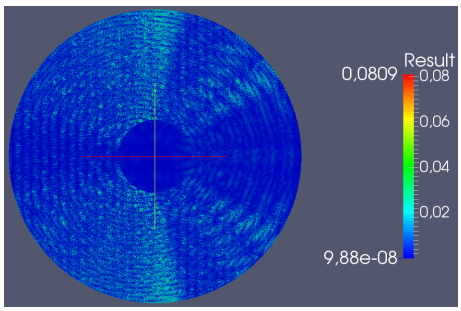

(b) Absolute error between the exact solution and the solution computed with HDG-$\mathbb{P}_2$ scheme, mesh M3.

Figure 5.27: Numerical solution, mesh M3, HDG-$\mathbb{P}_2$ scheme, V_x component.

The numerical convergence of the HDG method for this test problem is shown on fig. 5.28 and the one of the upwind DG method on fig. 5.29. As for the previous test problem, we observe that the two numerical convergences have the same behavior and that the optimal rate is not obtained for this test problem. The computational performances of both methods are summarized in tabs. 5.18 for the memory requirement and the number of non-zero terms in the global matrix, tab. 5.19 for the number of degrees of freedom and tab. 5.20 for the time required for the construction of the global matrix (in seconds) and for the resolution (in seconds). In tabs. 5.16-5.17 we present the mean and relative errors on V_x and σ_{xx} components for both methods.

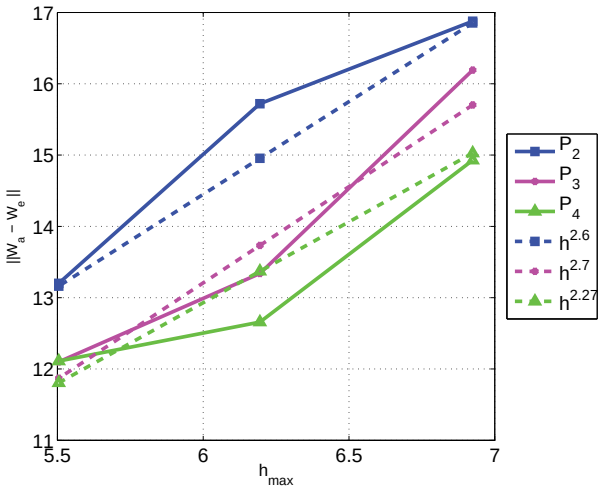

Figure 5.28: Numerical convergence order of the HDG method.

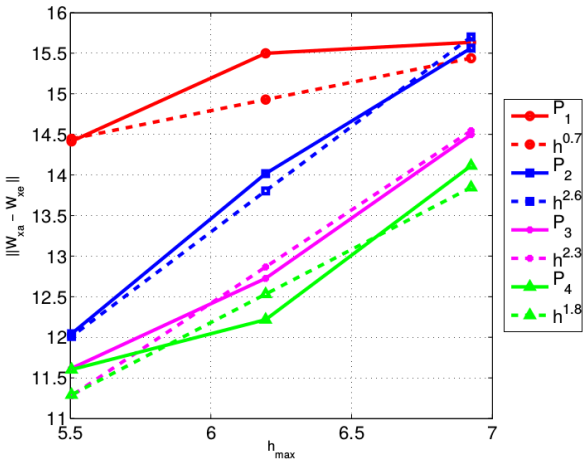

Figure 5.29: Numerical convergence order of the upwind DG method.

h (m)	Interpolation degree	Mean Error V_x		Relative Error V_x	
		HDG scheme	Upw. scheme	HDG scheme	Upw. scheme
1016.9	2	2.1	0.9	273.5	120.1
490.1	2	0.2	6.4e-02	91.5	31.0
245.9	2	5.0e-03	1.7e-03	9.6	3.3
1016.9	3	1.2	0.4	134.7	46.4
490.1	3	2.0e-02	1.4e-02	9.5	6.5
245.9	3	1.0e-03	9.9e-04	2.0	1.9
1016.9	4	0.4	0.3	42.0	29.9
490.1	4	7.3e-03	7.7e-03	3.4	3.6
245.9	4	9.9e-04	9.9e-04	1.9	1.9

Table 5.16: Mean and relative errors on V_x.

h (m)	Interpolation degree	Mean Error σ_{xx}		Relative Error σ_{xx}		Convergence order	
		HDG scheme	Upw. scheme	HDG scheme	Upw. scheme	HDG scheme	Upw. scheme
1016.9	2	7351.8	3742.9	213.2	108.6	-	-
490.1	2	457.8	143.2	52.3	16.4	1.6	2.1
245.9	2	9.1	5.5	4.1	2.5	3.7	2.9
1016.9	3	3141.9	1054.3	83.2	27.9	-	-
490.1	3	41.7	41.6	4.7	4.7	3.9	2.4
245.9	3	3.8	3.9	1.7	1.7	1.8	1.6
1016.9	4	838.6	667.3	22.1	17.6	-	-
490.1	4	25.5	26.9	2.9	3.0	3.1	2.6
245.9	4	3.8	3.8	1.7	1.7	0.8	0.9

Table 5.17: Mean and relative errors on σ_{xx} and convergence order.

# Mesh elements	Interpolation degree	Non-zeros terms		Memory (MB)	
		HDG scheme	Upw. scheme	HDG scheme	Upw. scheme
1300	2	4.1e+05	1.7e+06	48	307
5400	2	1.8e+06	7.5e+06	202	1543
22000	2	7.0e+06	3.0e+07	879	7318
1300	3	7.3e+05	3.8e+06	77	604
5400	3	3.1e+06	1.6e+07	351	3233
22000	3	1.2e+07	6.6e+07	1553	15741
1300	4	1.1e+06	7.3e+06	111	988
5400	4	4.9e+06	3.1e+07	526	5160
22000	4	1.9e+07	1.2e+08	2362	23982

Table 5.18: Number of non-zero terms in the global matrix and memory used.

# Mesh elements	Interpolation degree	# dof		#dof/wavelength	
		HDG scheme	Upw. scheme	HDG scheme	Upw. scheme
1300	2	1.1e+04	3.8e+04	6	19
5400	2	4.9e+04	1.6e+05	24	81
22000	2	2.0e+05	6.5e+05	98	325
1300	3	1.6e+04	6.3e+04	8	31
5400	3	6.5e+04	2.7e+05	32	135
22000	3	2.6e+05	1.1e+06	130	541
1300	4	1.9e+04	9.5e+04	10	47
5400	4	8.2e+04	4.1e+05	41	202
22000	4	3.3e+05	1.6e+06	163	812

Table 5.19: Total number degrees of freedom (ndof) and ndof by wavelength (λ_w) for both methods.

# Mesh elements	Interpolation degree	Construction time(s)		Solution time (s)	
		HDG scheme	Upw. scheme	HDG scheme	Upw. scheme
1300	2	0.2	4.7e-02	0.2	2.3
5400	2	0.9	0.2	1.1	14.4
22000	2	3.5	0.8	6.6	98.2
1300	3	0.6	0.1	0.3	5.1
5400	3	2.7	0.5	2.0	36.7
22000	3	11.1	1.9	13.7	348.1
1300	4	1.7	0.2	0.5	9.2
5400	4	7.2	1.0	3.4	69.6
22000	4	30.1	3.8	23.8	525.4

Table 5.20: Time required for the global matrix construction and for the system resolution.

6 Conclusion

In this report, we studied the HDG method for the 2D elastic Helmholtz equations. The convergence order of the HDG method is numerically optimal, as we have for classical finite elements. For the same accurancy, the HDG formulation uses less memory than nodal DG method, even if we have to use an interpolation order more with the HDG method than the nodal DG method or if we have to refine the mesh. For given mesh and interpolation order, the HDG method is more competitive in memory and computational time terms. These results have to be confirmed for parallel implementation and for the 3D elastic Helmholtz equations.

Acknowledgements

The authors acknowledge the support by the Inria-TOTAL strategic action DIP (dip.inria.fr).

References

[1] Robert M. Kirby and Spencer J. Sherwin. To CG or to HDG: A comparative study. *Journal of Scientific Computing*, 51:183–212, May 2011.

[2] B. Cockburn, J. Gopalakrishnan, and R. Lazarov. Unified hybridization of discontinuous Galerkin, mixed and continuous Galerkin methods for second order elliptic problems. *SIAM Journal on Numerical Analysis*, 47:1319–1365, 2009.

[3] N. C. Nguyen, J. Peraire, and B. Cockburn. High-order implicit hybridizable discontinuous Galerkin methods for acoustics and elastodynamics. *Journal of Computational Physics*, (230):3695–3718, 2011.

[4] Stéphane Lanteri, Liang Li, and Ronan Perrussel. Numerical investigation of a high order hybridizable discontinuous Galerkin method for 2d time-harmonic Maxwell's equations. *COMPEL*, 32(3):1112–1138, 2013.

[5] N.C. Nguyen, J. Peraire, and B. Cockburn. Hybridizable discontinuous Galerkin methods for the time-harmonic Maxwell's equations. *Journal of Computational Physics*, 230:7151–7175, 2011.

[6] N. C. Nguyen, J. Peraire, and B. Cockburn. An implicit high-order hybridizable discontinuous Galerkin method for linear convection-diffusion equations. *Journal of Computational Physics*, 228:3232–3254, 2009.

[7] N. C. Nguyen, J. Peraire, and B. Cockburn. An implicit high-order hybridizable discontinuous Galerkin method for nonlinear convection-diffusion equations. *Journal of Computational Physics*, 228:8841–8855, 2009.

[8] N. C. Nguyen and J. Peraire. Hybridizable discontinuous Galerkin methods for partial differential equations in continuum mechanics. *Journal of Computational Physics*, (231):5955–5988, 2012.

[9] Sarah Delcourte, Loula Fezoui, and Nathalie Glinsky-Olivier. A high order discontinuous Galerkin method for the seismic wave propagation. *ESAIM: Proceedings*, 27:70–89, May 2009.

[10] P.R. Amestoy, I.S. Duff, and J.-Y. L'Excellent. Multifrontal parallel distributed symmetric and unsymmetric solvers. *Computationnal Methods in Applied Mechanics and Engineering*, 184:501–520, 2000.

[11] Romain Brossier. *Imagerie sismique à deux dimensions des milieux visco-élastiques par inversion des formes d'ondes: développements méthodologiques et applications.* PhD thesis, Université de Nice-Sophia Antipolis, November 2009.

[12] Jean Virieux et al., Vincent Etienne et al., and Victor Cruz-Atienza et al. Modelling Seismic Wave Propagation for Geophysical Imaging. *Seismic Waves, Research and Analysis*, pages 253–304, 2012.

[13] Josep de la Puente, Martin Käser, Michael Dumbser, Heiner Igel, et al. An arbitrary high-order discontinuous Galerkin method for elastic waves on unstructured meshes - IV. Anisotropy. *Geophysical Journal International*, 169:1210–1228, 2007.

[14] Michael Dumbser and Martin Käser. An arbitrary high-order discontinuous Galerkin method for elastic waves on unstructured meshes - II; The three-dimensional isotropic case. *Geophysical Journal International*, 167:319–336, 2006.

[15] M. Ainsworth, P. Monk, and W. Muniz. Dispersive and Dissipative Properties of Discontinuous Galerkin Finite Element Methods for the Second-Order Wave Equation. *Journal of Scientific Computing*, 27(1-3):5–40, June 2006.

[16] S. Lanteri and M. El Bouajaji. High order discontinuous Galerkin method for the solution of 2D time-harmonic Maxwell's equations. *Applied Mathematics and Computation*, 219:7241–7251, 2013.

[17] Giorgio Giorgiani. *Adaptative Hybrid Discontinuous Methods For Fluid and Wave Problems*. PhD thesis, April 2013.

[18] Michel Kern. *Problèmes inverses: aspects numériques*. 2002-2003.

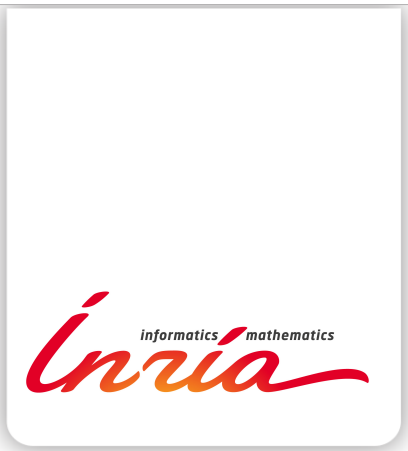

RESEARCH CENTRE
BORDEAUX – SUD-OUEST

200 avenue de la Vieille Tour
33405 Talence Cedex

Publisher
Inria
Domaine de Voluceau - Rocquencourt
BP 105 - 78153 Le Chesnay Cedex
inria.fr

ISSN 0249-6399